infection, we assume that HIV and immune dynamics can be considered at a steady state after the acute infection.

We calculate the CD4$^+$ T cell number, virus load of HIV, and CTL activity at a possible equilibrium in Fig. 2 using the average values of the parameters λ, d, β, and a among 10 patients in Table 1. The black and red solid lines, respectively, represent cell numbers at the controlled and immunodeficiency state over HIV infection (black dashed lines represent cell numbers at E_c^-).

(i) When viral infectivity (i.e., infection rate of HIV: β) is remarkably large, in the sense that $\lambda c/b<\beta$, our immune system does not establish CTL responses in spite of a very high viral load (Fig. 2(i): we used 100-fold viral infectivity β to satisfy with $\lambda c/b<\beta$). Too many CD4$^+$ T cells are destroyed during the acute infection. Therefore, infected individuals immediately develop immunodeficiency without an asymptomatic phase (Binley et al., 2000; Cecilia et al., 1999; Meissnera et al., 2004). An example for rapid disease progression is observed in experimental SIV/SHIV infection (Binley et al., 2000; Kozyrev et al., 2001).

On the other hand, when the viral infectivity is small, in the sense that $\lambda c/b>\beta$, our immune system can establish sustained CTL responses. In this case, the disease progression dynamics is determined by the following cytopathogenic thresholds:

$$a_- = \frac{\lambda\beta}{d} - \frac{\beta\sqrt{\lambda c b\beta}}{cd}, \quad \bar{a} = \frac{\lambda\beta}{d} - \frac{b\beta^2}{cd}.$$

Therefore, (ii) when the cytopathogenicity (i.e., death rate of infected CD4$^+$ T cells) is small, in the sense that $0<a<a_-$, the sustained CTLs suppress HIV replication for a long time after the acute infection (Fig. 2(ii)). However, as the immune impairment rate increases, the CTL responses weaken gradually and the infected individuals eventually develop AIDS because of depletion of CD4$^+$ T cells. This progressive immune decline corresponds to the typical disease progression of HIV infection (Janewa et al., 2004). Over the disease progression, we have the following two immune impairment thresholds which can determine patients' symptoms:

$$\bar{\varepsilon} = \frac{ac}{b\beta} + \frac{a\beta}{ad-\lambda\beta}, \quad \varepsilon_- = \frac{(\sqrt{b\beta}-\sqrt{\lambda c})^2}{bd}.$$

Until the impairment rate exceeds $\bar{\varepsilon}$, CTLs control the virus load at a very low level. However, if the impairment rate exceeds this threshold value, the patients risk development of AIDS because both the controlled and immunodeficiency states can be stable simultaneously (see Appendix). Stochastic perturbation in patients caused by virological and immunological events might change the patients' state from the controlled state to the immunodeficiency state (Iwami et al., in revision). Here we call $\bar{\varepsilon}$ the "risky threshold". By evaluating the eigenvalues at E_u and E_c^- in detail, we can show that the risky threshold corresponds to a transcritical bifurcation point (see Appendix). Moreover, once the impairment rate becomes greater than ε_-, our immune system collapses completely, the CTL responses become inactivated, and the patients always develops AIDS. This is true because the controlled equilibrium is degenerated, but the immunodeficiency equilibrium remains stable. We designate ε_- as the "immunodeficiency threshold". By evaluating the eigenvalues at E_c^- and E_c^+ in detail, we can show that the immunodeficiency threshold corresponds to a saddle-node bifurcation point (see Appendix). We investigate this typical disease progression in detail later.

Furthermore, when cytopathogenicity is not small ((iii) $a_-<a<\bar{a}$ or (iv) $\bar{a}<a<a_{max}$), CTL responses are slight or nonexistent because of the lack of antigen signals (see Figs. 2(iii) and (iv): we used adjusted cytopathogenicities a, which can be satisfied, respectively, with $a_-<a<\bar{a}$ and $\bar{a}<a<a_{max}$). Here we mention that $a_{max} = \lambda\beta/d$ is derived from the assumption that $R_0>1$. Actually, even if CTL responses are not induced, the viral load remains at a very low level in both cases (therefore, a slight immune response eventually becomes inactivated in case (iii)). These phenomena are considered as CTL non-responsiveness, which differs from the immunodeficiency associated with HIV infection (Wodarz et al., 1998) (AIDS is characterized by a high virus load of HIV and CD4$^+$ T cell depletion, Janewa et al., 2004). The CTL non-responsiveness might be observed in a viral infection with a high degree of cytopathogenicity, but it is inapplicable to HIV infection.

3.3. A progressive risk of immunodeficiency in HIV infection

We investigate a progressive risk of immunodeficiency by evaluating a basin of attraction of the immunodeficiency state and provide a detailed explanation of the typical disease progression. Here we also assume that the parameters λ, d, β, and a are the average values of 10 patients in Table 1. Then the risky and immunodeficiency thresholds to $\bar{\varepsilon} = 303.63$ and $\varepsilon_- = 1366.45$ are estimated, respectively.

In Fig. 3, we plot a basin of attraction (i.e. absorbing region) of immunodeficiency state E_u on x–z space with $y = y_u = 0.244$ as a red region and call it the "risky zone". Therefore, if their virological and immunological states are located in the risky zone, HIV patients eventually develop immunodeficiency (i.e., all

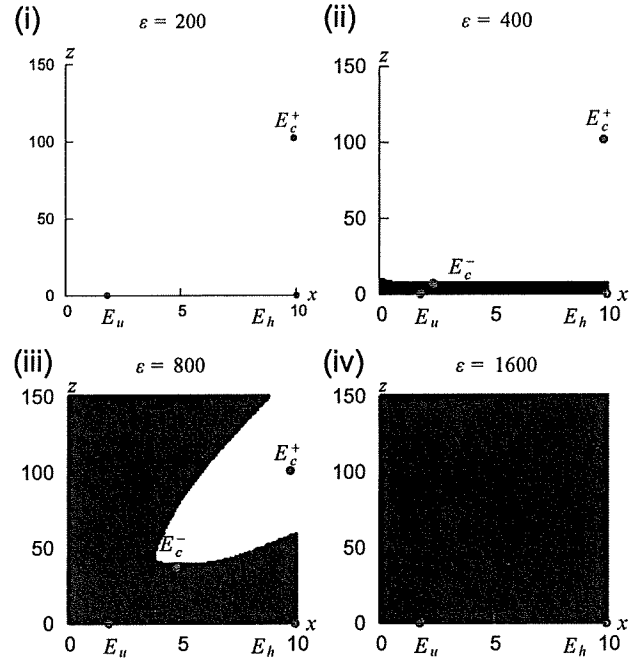

Fig. 3. Risky zone of immunodeficiency: we plot a basin of attraction of E_u as a red region and call it a "risky zone". For (i), until the immune impairment rate (ε) exceeds the risky threshold ($\bar{\varepsilon}$), only E_c^+ is stable. On the other hand, with (ii), when the impairment rate exceeds the risky threshold, E_c^- is generated into $\mathbb{R}_+^3$ via a transcritical bifurcation with E_u and the risky zone emerges (i.e., both E_c^+ and E_u become stable simultaneously). The stable manifold of E_c^- forms a boundary surface of the risky zone. Furthermore, in (iii), the risky zone expands during the impairment rate increases until the immunodeficiency threshold (ε_-). However, in (iv), once the impairment rate becomes greater than the immunodeficiency threshold, $E_c^\pm$ are degenerated via a saddle-node bifurcation and the full space becomes the risky zone (i.e. only E_u is stable). Here the risky and immunodeficiency thresholds to $\bar{\varepsilon} = 303.63$ and $\varepsilon_- = 1366.45$ are estimated, respectively. (For interpretation of the references to color in this figure legend, the reader is referred to the web version of this article.)

orbits converge to E_u if their initial values are chosen from the risky zone).

We assume that the respective activated and infected $CD4^+$ T cell dynamics have already converged to the shortage state E_u during primary expansion and differentiation of CTLs in the acute infection. The immune impairment rate is low at the beginning of the infection. Therefore, sustained CTL responses are established; therefore, the viral replication is suppressed at a low level in the stable controlled state E_c^+ after the CTL naives begin to expand and differentiate (Fig. 3(i)). Consequently, the virus load of HIV equilibrates and remains at a virological set point immediately after the acute infection (Janewa et al., 2004; McMichael and Rowland-Jones, 2001). Here we remark that the shortage state E_u is stable in x–y space but is unstable in all space if ε is small, which implies that convergent steady state of model (1) always transfers from E_u to E_c^+ if z becomes positive. Furthermore, even if the immune impairment rate increases, the viral replication is well controlled by CTL responses at E_c^+ until the rate exceeds the risky threshold (i.e., $0<\varepsilon<\bar{\varepsilon}$). Actually, the immune suppression is robust for any stochastic perturbation because only E_c^+ is stable.

On the other hand, when the impairment rate becomes greater than the risky threshold (i.e., $\bar{\varepsilon}<\varepsilon$), the shortage state becomes the immunodeficiency state (i.e., E_u becomes stable in all space, which differs qualitatively from the shortage state) and the risky zone emerges (Fig. 3(ii)). Therefore, patients have a risk of development of immunodeficiency because stochastic perturbations caused by virological and immunological events, such as mutational changes of viral epitopes and their specific immune responses (McKnight and Clapham, 1995; McMichael and Rowland-Jones, 2001; Nowak and May, 2000), a switch of coreceptor from CCR5 to CXCR4 (Janewa et al., 2004), and an emergence of drug resistance (Richman, 2001) might drive patients from the controlled state E_c^+ to the risky zone (Iwami et al., in revision). Furthermore, the risky zone expands gradually (Fig. 3(iii)) as the impairment rate increases until the immunodeficiency threshold ($\varepsilon<\varepsilon_-$) is reached. Therefore, the risk is increased progressively. Consequently, the patients become sensitive to these stochastic perturbations.

However, once the impairment rate exceeds the immunodeficiency threshold ($\varepsilon_-<\varepsilon$), the risky zone expands into total space and the patients always develop AIDS (Fig. 3(iv)) because the immunodeficiency state E_u becomes a unique stable steady state, implying that a complete breakdown of the immune system occurs and that CTL responses no longer become re-activated.

Consequently, even if viral replication can be suppressed by CTLs at the virological set point immediately after the acute infection (Fig. 3(i)), as the immune impairment rate increases, patients tend to confront the risk of development of immunodeficiency (Fig. 3(ii)); that risk gradually increases (Fig. 3(iii)). They eventually develop AIDS (Fig. 3(iv)).

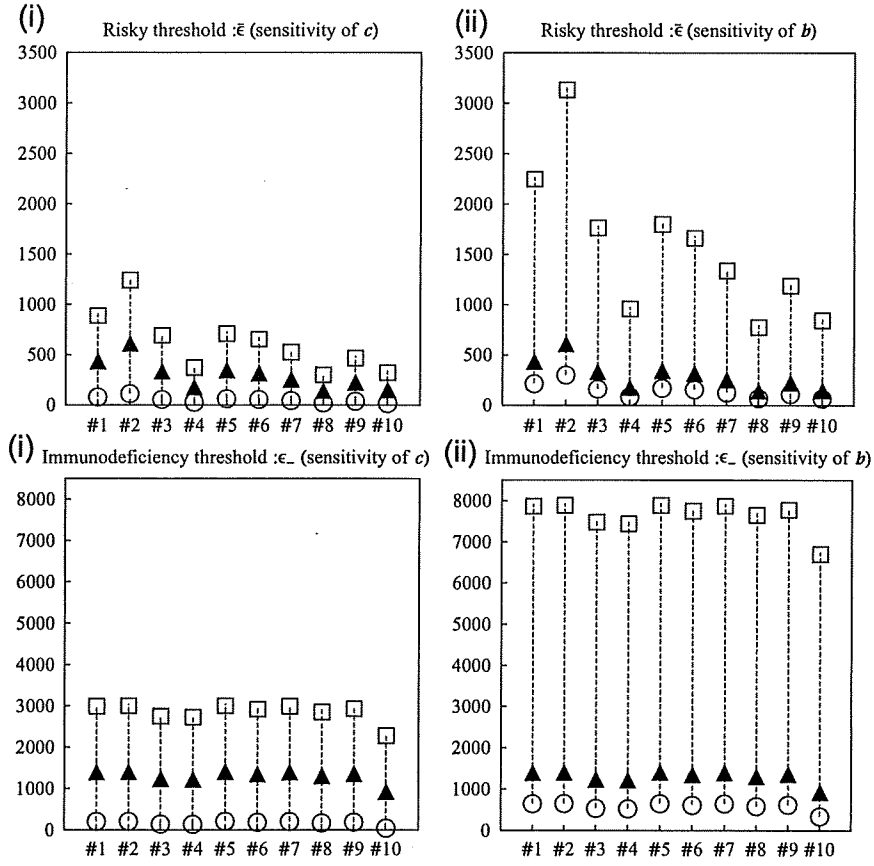

Fig. 4. Distribution of risky and immunodeficiency thresholds among 10 patients: we perform sensitivity analysis for variations in the immune impairment thresholds among 10 patients with respective ranges of (i) the proliferation rate and (ii) the decay rate of CTLs in Table 1. The colored triangle (▲) represents threshold values with the estimated parameter values. The colorless square (□) and circle (○), respectively, represent the maximum and minimum threshold values within the ranges. We confirm that all patients have their risky and immunodeficiency thresholds in close ranges, irrespective of virological and immunological differences. These cross-sectional studies based on our mathematical model predict the possible existence of the immune impairment thresholds in HIV infection.

3.4. Immune impairment thresholds in patients

Using our baseline parameter values and ranges in Table 1, we investigate the existence of risky and immunodeficiency thresholds among 10 patients and their cross-sectional distributions.

For an arbitrary value between the CTL proliferation (decay) rate c (b) in Table 1, the viral infectivity and the cytopathogenicity of each patient are satisfied, respectively, with $\lambda c/b > \beta$ and $0 < a < a_-$. For that reason, all patients take on typical disease progression, which implies that all patients have risky and immunodeficiency thresholds. We perform sensitivity analysis in Fig. 4 for variations in the immune impairment thresholds among 10 patients with respective ranges of (i) the proliferation rate and (ii) the decay rate of CTLs in Table 1 because these parameter values are not estimated from virus concentration data of the patients in Stafford et al. (2000) (we remark that, because these thresholds are independent of the killing rate of infected $CD4^+$ T cells p, we need not investigate their range). The colored triangle (▲) represents threshold values with estimated parameter values. The colorless square (□) and circle (○), respectively, represent the maximum and minimum threshold values within the ranges.

Fig. 4 portrays that the distributions of risky and immunodeficiency thresholds (particularly, the maximum values of risky thresholds) are more sensitive to the CTL decay rate than to its proliferation rate. However, risky and immunodeficiency thresholds among 10 patients seem to be distributed in close ranges in Fig. 4, irrespective of virological and immunological differences (threshold values with the estimated parameter values (▲) are distributed almost uniformly), which might imply that all patients tend to have a risk of development of AIDS with a close timing and that they eventually develop AIDS in a close range of the impairment rate (actually, in terms of our mathematical model, the length of asymptomatic phase is characterized by the wide shape of its distribution and the development is stochastic once the impairment rate exceeds the risky threshold, Iwami et al., in revision). These cross-sectional studies based on our mathematical model predict the possibility of the existence of immune impairment thresholds in HIV infection. Therefore, our theoretical framework of immune impairment effects over HIV infection might provide clear insight into the time when patients develop AIDS (i.e., a prediction of AIDS development).

4. Discussion

The onset of AIDS is characterized by a breakdown of the immune system after a long asymptomatic period (Janewa et al., 2004; McMichael and Rowland-Jones, 2001; Tunetsugu-Yokota, 2005). The mechanistic basis of this disease progression has remained obscure, but many researchers have sought to explain it. For example, in early models of HIV infection (Nowak and May, 2000), an explosion in the virus load caused by increased HIV variants' diversity explains the immune system collapse. In Wodarz et al. (1998), the CTL exhaustion induced by an evolutionary increase of viral infectivity accounts for immunodeficiency. Moreover, in Galvani (2005), the functional deterioration of T and B cells caused by accumulations of deleterious mutations is considered as a reason for development of AIDS. Consequently, to date, several approaches have been proposed to explain the progression of HIV infection to AIDS (Altes et al., 2003; De Boer and Boerlijst, 1994; Galvani, 2005; Hogue et al., 2008; Iwami et al., 2008; Nowak and May, 2000; Wodarz et al., 1998).

This paper presents discussion of an immune impairment effect caused by the depletion and dysfunction of DC on HIV disease progression. Because the progressive decrease of DC number and function during the course of HIV-1 infection is observed (Donaghy et al., 2001, 2003; Macatonia et al., 1990), we simply assumed that the immune impairment rate (ε) increases over the HIV infection instead of considering the population dynamics of DCs directly (in contrast, in Hogue et al., 2008, to investigate the dual role of DCs (i.e. transmission of HIV and activation of immune cell), the population dynamics of DCs are involved into their model). We also remark that the immune impairment effects included in our model (1) arose from many other sources. For example, during HIV infection, programmed death 1 (PD-1) expression is elevated on HIV-specific $CD8^+$ T cells (Freeman et al., 2006) and engagement of PD-1 by its ligands (PD-L) inhibits several $CD8^+$ T cell functions (Barber et al., 2006) (actually, blocking the PD-1–PD-L pathway engenders increased T cell proliferation and effector cytokine production, Velu et al., 2009). The immune impairment effect driven from the PD-1–PD-L pathway also impairs CTL responses. Therefore, the effect can be described by our mathematical model. Consequently, our model is applicable to other immune impairment phenomena in HIV infection.

Results show that the patterns of disease progression of our model (1) are divided into four cases (Fig. 2). In typical disease progression, which is characterized by a low infection rate (β) and cytopathogenicity of HIV (a), we derived two immune impairment thresholds: the risky threshold ($\bar{\varepsilon}$) and the immunodeficiency threshold (ε_-) (Fig. 2(ii)). Until the immune impairment rate exceeds the risky threshold, CTLs are induced and suppress viral replication (Fig. 3(i)), but once the impairment rate becomes greater than the threshold, the infected individuals face the risk of development of immunodeficiency (Figs. 3(ii)–(iii)). Furthermore, if the impairment rate becomes greater than the immunodeficiency threshold, then patients always develop AIDS (Fig. 3(iv)). Consequently, our theoretical framework can explain disease progression: many experimenters have concluded that the progressive alteration of the immune system (the depletion and dysfunction of DCs are central to many of these hypotheses) might result from the development of AIDS (Donaghy et al., 2001, 2003; Kawamura et al., 2003; Lore et al., 2002; Macatonia et al., 1990; Patterson et al., 1998; Smed-Sorensen et al., 2004; Wu and Kewal-Ramani, 2006).

The central description of the development of AIDS in our model (1) is a catastrophic change of the patients' state (e.g., immunodeficiency characterized by the CTL exhaustion proposed in Wodarz et al., 1998) (Figs. 2 and 3). The mechanistic basis of the catastrophe is derived from the bistability of controlled state E_c^+ and immunodeficiency state E_u. Actually, in several models, a bistability of steady states has been discussed to explain, for example, the multiple virological set points (Altes et al., 2003), the explosion of virus load (De Boer and Boerlijst, 1994), and CTL exhaustion (Wodarz et al., 1998). A readily apparent difference of our model (1) from these earlier models is the consideration of the progressive immune impairment effect which depends on the number of infected $CD4^+$ T cells. Furthermore, we were able to estimate various thresholds related to immunodeficiency strictly. Although qualitatively similar results were obtained through more complex models (Altes et al., 2003; De Boer and Boerlijst, 1994; Wodarz et al., 1998; Wodarz and Nowak, 1999), which can be treated analytically only to a slight degree, one important result of our model is the clear and simple concept illustrating the risk of immunodeficiency.

We also investigated the distribution of risky and immunodeficiency thresholds among 10 patients. It is particularly interesting that we showed that all patients follow the typical disease progression and that the risky and immunodeficiency thresholds are distributed in close ranges, irrespective of virological and immunological differences (Fig. 4). Here we must mention that our baseline parameter values and ranges in Table 1 could not be

justified completely. In Fig. 5 which represents time-course of virus population for 2000 days, we check how our mathematical model fits the 10 patients' virus concentration data using our baseline parameter values in Table 1. The red dots during the acute infection in each panel represent the patient data which were used in parameter estimation in Stafford et al. (2000) and the black dots after the acute infection represent the data which were not used in the parameter estimation. We assumed that, for example, because of a time delay of immune response (Janewa et al., 2004), CTL responses are induced after 30 days from the

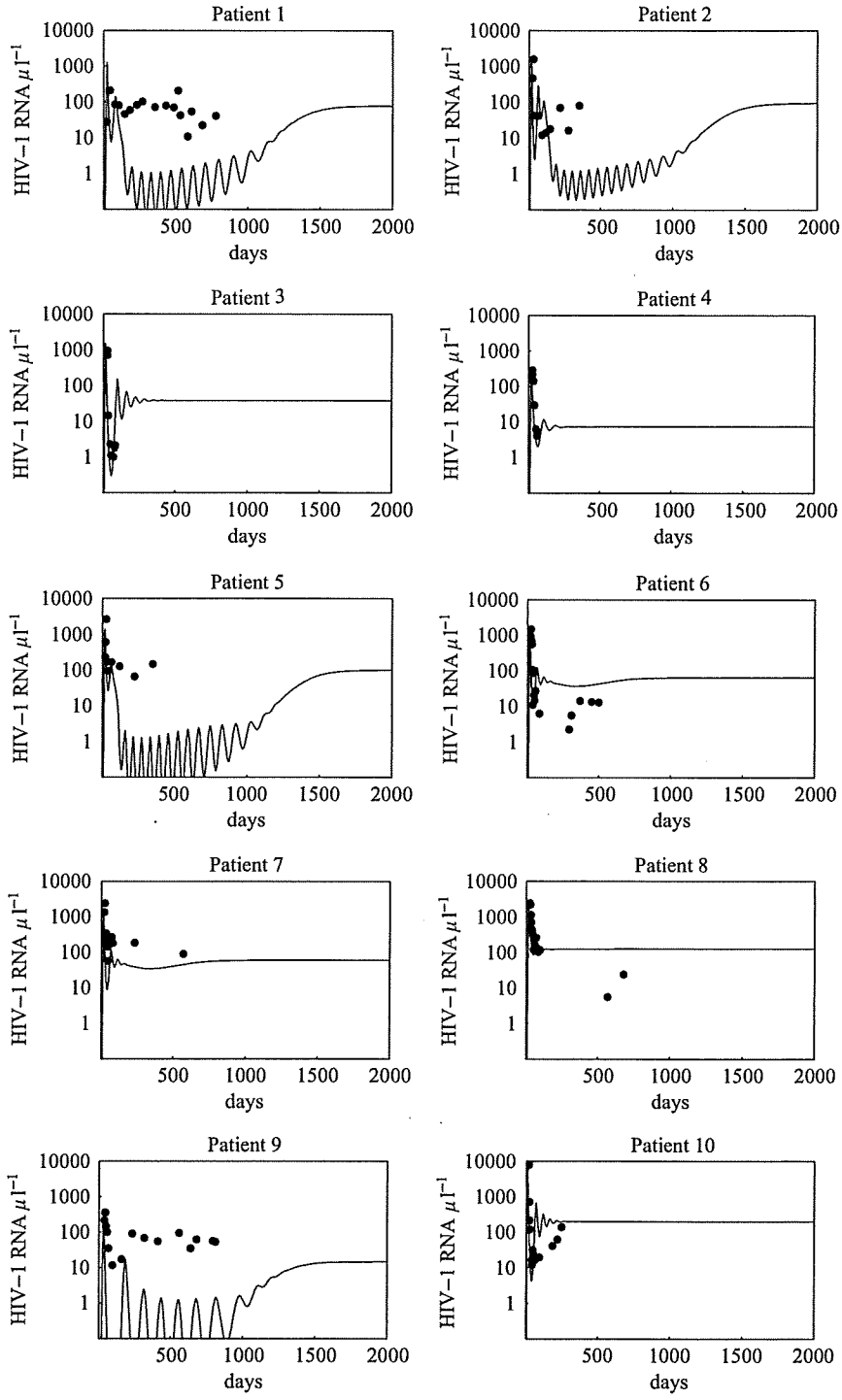

Fig. 5. Fit test for 10 patient data: we investigate how our mathematical model fits the 10 patients' virus concentration data using our baseline parameter values in Table 1. Both the red and black dots represent patient data but only the red dots were used in parameter estimation in Stafford et al. (2000). Here we calculate the virus population (HIV-1 RNA μl^{-1}) from $y(t)$ using original estimated parameter values in Stafford et al. (2000) (we define $v(t) = \pi y(t)/c$ where π and c are the notation used in Stafford et al. (2000)). (For interpretation of the references to color in this figure legend, the reader is referred to the web version of this article.)

date of initial HIV infection ($z(t)=0$ for $0\le t<30$ and $z(30)>0$) and that, because of progressive depletion and dysfunction of DC (Donaghy et al., 2001, 2003; Macatonia et al., 1990), the immune impairment accumulates with a very low rate during disease progression, $\varepsilon(t)=1.5(t-30)$, where 1.5 is the rate of average impairment per day (we do not know how the impairment rate ε can be formulated but we use a simplest formulation of increasing function). We found that our model and baseline parameter values fit the patient data in the short-term (red dots) but hardly fit that in the long-term (black dots). In particular, in patients 1, 2, 5, and 9, different dynamical behaviors (for example, our model predicts the oscillations which are not seen in data) are observed between the Stafford model and our model (we find in patients 3, 4, 6, 7, 8, and 10, similar dynamical behaviors although our model includes the immune cell dynamics). This is because the parameter values of λ, d, β, and a are derived from the short-term data (i.e., red dots), the number of activated $CD4^+$ T cells (10 cells per μl of peripheral blood) and the decay rate of HIV ($3\,day^{-1}$ which is referred to Perelson et al., 1996) were assumed to be the same value among 10 patients in Stafford et al. (2000). Moreover, we estimated the immunological parameter values of p, c, b separately using previously estimated parameter values in Davenport et al. (2004), Mandl et al. (2007) and Ogg et al. (1999) and these parameter values were also assumed to be the same among 10 patients. That is, the parameters in Table 1 are not consistent with the data and might not be adequate to long-term dynamics of our model. In order to predict the long-term virus population dynamics of the patients by our model, we have to use the parameter values estimated by using a long-term data. Therefore, these simplifications of estimation of the parameters might engender some gap in the distribution and the time-course of virus population. Nevertheless, although we must estimate the exact parameter values of the 10 patients, our cross-sectional studies imply the possible existence of immune impairment thresholds in HIV infection and validity of our theory.

In summary, our results imply that recovering DC function and increasing DC number might be effective for inducing immune response and delaying the disease progression (actually, several studies of DC immunotherapy found a transient decrease of the virus load by activating T cell responses against HIV-1, Connolly et al., 2008; Garcia et al., 2005; Rinaldo, 2008) because the modulation of DC engenders a decrease of the immune impairment rate (ε); following such a strategy, the risky zone dwindles or disappears (see Fig. 3). The findings described herein present important implications for the design of therapeutic vaccines. For example, reconstitution of CD80/CD86 expression in DC, which reduces the impairment effect, might be important to consider development of therapeutic HIV-1 vaccine (Lore et al., 2002). In addition, if the impairment rate can be quantified using some data, our theory might enable prediction of the timing of AIDS development. Consequently, although our model presents several limitations because of its simplification of estimation of the parameter and its neglect of population dynamics of DCs, our study points out that further experimental investigation of DC depletion and dysfunction in patients and quantification of the immune impairment rate will be important for understanding of HIV disease progression and for development of DC vaccines and prediction of AIDS.

Acknowledgments

The authors express their appreciation to Prof. X. Liu and Prof. W. Wang for valuable comments. We would also like to thank anonymous referees for very helpful suggestions and comments, which have improved the quality of our study. S. Iwami was supported by Research Fellowships of the Japan Society for the Promotion of Science for Young Scientists. S. Nakaoka was supported by (i) Research Fellowships of the Japan Society for the Promotion of Science for Young Scientists and (ii) the Sasakawa Scientific Research Grant from The Japan Science Society.

Appendix A. Mathematical analysis

The model has four possible equilibria:

$E_h=(x_h,0,0)$, $E_u=(x_u,y_u,0)$, $E_c^-=(x_c^-,y_c^-,z_c^-)$,

$E_c^+=(x_c^+,y_c^+,z_c^+)$.

Here $x_h=\lambda/d$, $x_u=a/\beta$, $y_u=(\lambda-dx_u)/\beta x_u$. Furthermore, $x_c^\pm$, $y_c^\pm$, $z_c^\pm$, respectively, signify the roots of the following equations:

$$f(x)=cdx^2+(b\beta-\varepsilon bd-\lambda c)x+\lambda\varepsilon b=0,$$

$$g(y)=\varepsilon b\beta y^2+(b\beta+\varepsilon bd-\lambda c)y+bd=0,$$

$$h(z)=cdp^2z^2+p\{2acd+\beta(b\beta-\lambda c-\varepsilon bd)\}z+a^2dc+a\beta(b\beta-\varepsilon bd-\lambda c)+\varepsilon\lambda\beta^2b=0.$$

The basic reproductive number for one infected cell is definable as $R_0=\lambda\beta/ad$, which represents the average number of cells infected by a single infected cell in an otherwise susceptible cell population (Nowak and May, 2000).

Clearly, E_h always exists and E_u exists if and only if $R_0>1$. Next we consider the existence condition of $E_c^\pm$. Because the discriminants for the above three functions f, g, and h are the same and given as $D=D_f=D_g=D_h=\varepsilon^2b^2d^2-2bd(b\beta+\lambda c)\varepsilon+(b\beta-\lambda c)^2$, we can obtain

$$D>0 \iff \varepsilon<\frac{(\sqrt{b\beta}-\sqrt{\lambda c})^2}{bd}=\varepsilon_- \quad \text{or} \quad \varepsilon>\frac{(\sqrt{b\beta}+\sqrt{\lambda c})^2}{bd}=\varepsilon_+.$$

From $f(0)>0$ and $g(0)>0$, the following relations hold:

(A) $x_c^\pm>0 \iff D>0,\quad b\beta-\varepsilon bd-\lambda c<0,$

(B) $y_c^\pm>0 \iff D>0,\quad b\beta+\varepsilon bd-\lambda c<0.$

If $\lambda c-b\beta<0$, then we have $y_c^\pm<0$ from the last inequality in (B), which implies that $E_c^\pm$ cannot exist in $\mathbb{R}^3_+$. Hereinafter we assume that $\lambda c-b\beta>0$. We define $\varepsilon_0=(\lambda c-b\beta)/bd$. Then the last inequality in (A) is satisfied for any $0<\varepsilon$ and the last inequality in (B) is satisfied for $0<\varepsilon<\varepsilon_0$. Because $0<\varepsilon_-<\varepsilon_0$, we have $x_c^\pm>0$ and $y_c^\pm>0$ iff $0<\varepsilon<\varepsilon_-$. For $h(z)=0$, we have two cases: (i) $h(0)<0$ and (ii) $h(0)>0$. In case (i) of $h(0)<0$, it is clear that $z_c^-<0$ and $z_c^+>0$. If (a) $ad-\lambda\beta>0$ (i.e. $R_0<1$), we can show that

$$\begin{aligned}\overline{\varepsilon}>\varepsilon_+ &\iff \frac{ac}{b\beta}+\frac{a\beta}{ad-\lambda\beta}>\frac{(\sqrt{b\beta}+\sqrt{\lambda c})^2}{bd}\\ &\iff cd^2a^2-2d\beta\sqrt{\lambda c}(\sqrt{b\beta}+\sqrt{\lambda c})a+\lambda\beta^2(\sqrt{b\beta}+\sqrt{\lambda c})^2>0\\ &\iff \{ad\sqrt{c}-\beta\sqrt{\lambda}(\sqrt{b\beta}+\sqrt{\lambda c})\}^2>0.\end{aligned}$$

Here, $\overline{\varepsilon}=ac/b\beta+a\beta/(ad-\lambda\beta)$, which satisfies $h(0)|_{\varepsilon=\overline{\varepsilon}}=0$. Therefore, we can obtain that

$ad-\lambda\beta>0,\quad h(0)<0 \iff \varepsilon>\overline{\varepsilon},\quad \overline{\varepsilon}>\varepsilon_+.$

If (b) $ad-\lambda\beta<0$ (i.e., $R_0>1$), we can also show that

$ad-\lambda\beta<0,\quad h(0)<0 \iff \varepsilon<\overline{\varepsilon},\quad \overline{\varepsilon}<\varepsilon_-.$

Therefore, we can conclude that if $ad-\lambda\beta>0$, then $E_c^\pm$ cannot exist in $\mathbb{R}^3_+$ (see Fig. 6(a)). If $ad-\lambda\beta<0$, then we have two

intervals of a: $0<a<\bar{a}$ and $\bar{a}<a<a_{max}$. Here $\bar{a}$ satisfies $\bar{\varepsilon}(\bar{a})=0$. When $0<a<\bar{a}$ (i.e., $0<\bar{\varepsilon}$), then $E_c^{\pm}$ can exist under $0<\varepsilon<\bar{\varepsilon}$ and E_c^{-} cannot exist in $\mathbb{R}^3_+$ (see Fig. 6(b)). However, when $\bar{a}<a<a_{max}$ (i.e., $\bar{\varepsilon}<0$), $E_c^{\pm}$ cannot exist in $\mathbb{R}^3_+$ for any $\varepsilon>0$ (see Fig. 6(b)). For the case (ii) $h(0)>0$, it seems clear that $z_c^{\pm}>0$ if $\beta(\lambda c+\varepsilon bd-b\beta)-2acd>0$ and $D>0$. The following relation holds:

$$\beta(\lambda c+\varepsilon bd-b\beta)-2acd>0 \iff \varepsilon>\frac{2ac}{b\beta}+\frac{b\beta-\lambda c}{bd}=\varepsilon_m.$$

Next, we let $G(a)$ denote

$$G(a)=\bar{\varepsilon}-\varepsilon_m=-\frac{ac}{b\beta}+\frac{a\beta}{ad-\lambda\beta}+\frac{\lambda c-b\beta}{bd}.$$

In fact, $G'(a)<0$, $G(0)>0$, $\lim_{a\to\infty}G(a)=-\infty$ and $\lim_{a\to a_{max}\pm 0}G(a)=\pm\infty$ (see Fig. 7). This implies that there exist $a_{\pm}$ such that $G(a_{\pm})=0$ (i.e., $\bar{\varepsilon}=\varepsilon_m$). In fact, we have

$$G(a_{\pm})=0 \iff a_{\pm}=\frac{\lambda\beta}{d}\pm\frac{\beta\sqrt{\lambda cb\beta}}{cd}.$$

Therefore, if $0<a<a_-$ or $a_{max}<a<a_+$, then $\bar{\varepsilon}>\varepsilon_m$: otherwise $\bar{\varepsilon}<\varepsilon_m$ (see Fig. 7(i)). In addition, for ε_m, it can be shown that $\varepsilon_m(a_-)=\varepsilon_-$. Consequently, if $0<a<a_-$, then $\varepsilon_m<\varepsilon_-$; otherwise $\varepsilon_m>\varepsilon_-$ (see Fig. 7(ii)). Similarly, we can obtain the following relations for (a) $ad-\lambda\beta>0$ and (b) $ad-\lambda\beta<0$:

$$ad-\lambda\beta>0,\quad h(0)>0 \iff \varepsilon<\bar{\varepsilon},\quad \bar{\varepsilon}>\varepsilon_+,$$

$$ad-\lambda\beta<0,\quad h(0)>0 \iff \varepsilon>\bar{\varepsilon},\quad \bar{\varepsilon}<\varepsilon_-.$$

We can therefore conclude the following: if $ad-\lambda\beta>0$ (i.e., $a_{max}<a<a_+$ or $a_+<a$), then $E_c^{\pm}$ cannot exist in $\mathbb{R}^3_+$ (see Fig. 8(a)). Furthermore, if $ad-\lambda\beta<0$, then we have two intervals of a: $0<a<a_-$ and $a_-<a<a_{max}$ (see Fig. 8(b)). When $0<a<a_-$, $E_c^{\pm}$ can exist in $\mathbb{R}^3_+$ under $\bar{\varepsilon}<\varepsilon<\varepsilon_-$, but when $a_-<a<a_{max}$, $E_c^{\pm}$ cannot exist in $\mathbb{R}^3_+$.

Hereinafter, we explain the stability of these equilibria in detail. From a direct calculation, the eigenvalues of $J(E_h)$ are $-d$, $-b$ and βx_h-a, where J is the Jacobian matrix of (1), which implies that if $R_0<1$, then E_h is stable; otherwise E_h is unstable. The Jacobian matrix of (1) at E_u is

$$J(E_u)=\begin{bmatrix}-d-\beta y_u & -\beta x_u & 0\\ \beta y_u & 0 & -py_u\\ 0 & 0 & \dfrac{cx_uy_u}{1+\varepsilon y_u}-b\end{bmatrix}.$$

We can readily confirm that the first 2×2 block is stable. Therefore, the stability of E_u is determined by the sign of eigenvalue $cx_uy_u/(1+\varepsilon y_u)-b$. We can conclude that

$$\frac{cx_uy_u}{1+\varepsilon y_u}-b<0 \iff h(0)>0.$$

As stated earlier, $h(0)>0$ and $R_0>1$ are equivalent to $\bar{\varepsilon}<\varepsilon$. That is, if $\bar{\varepsilon}<\varepsilon$, then E_u is stable; otherwise E_u is unstable. The Jacobian matrix of (1) at $E_c^{\pm}$ is

$$J(E_c^{\pm})=\begin{bmatrix}-d-\beta y_c^{\pm} & -\beta x_c^{\pm} & 0\\ \beta y_c^{\pm} & 0 & -py_c^{\pm}\\ \dfrac{cy_c^{\pm}z_c^{\pm}}{1+\varepsilon y_c^{\pm}} & \dfrac{cx_c^{\pm}z_c^{\pm}}{(1+\varepsilon y_c^{\pm})^2} & 0\end{bmatrix}.$$

The characteristic equation of $J(E_c^{\pm})$ is

$$s^3+a_1s^2+a_2s+a_3=0,$$

where

$$a_1=d+\beta y_c^{\pm},\quad a_2=\beta^2x_c^{\pm}y_c^{\pm}+\frac{pcx_c^{\pm}y_c^{\pm}z_c^{\pm}}{(1+\varepsilon y_c^{\pm})^2},$$

$$a_3=\frac{pcx_c^{\pm}y_c^{\pm}z_c^{\pm}}{1+\varepsilon y_c^{\pm}}\left(\frac{d+\beta y_c^{\pm}}{1+\varepsilon y_c^{\pm}}-\beta y_c^{\pm}\right).$$

Here s denotes the indeterminate of the polynomial. Therefore, from the Routh–Hurwitz criterion, all eigenvalues have negative real parts if and only if

$$a_1>0,\quad a_3>0,\quad a_1a_2-a_3>0.$$

Clearly, $a_1>0$ and $a_1a_2-a_3>0$. Therefore, the stability of $E_c^{\pm}$ is determined by the sign of a_3. We can show

$$a_3>0 \iff \frac{d}{\beta\varepsilon}>y_c^{\pm 2}.$$

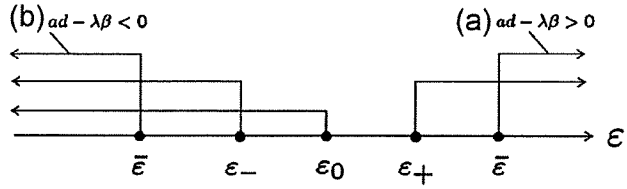

Fig. 6. Graphical presentation of existence conditions for $E_c^{\pm}$ with $h(0)<0$.

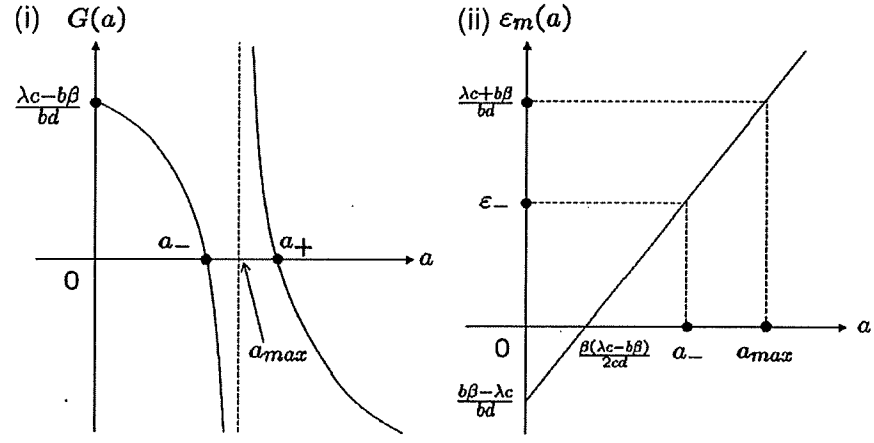

Fig. 7. Graphical presentation of $G(a)$ and $\varepsilon_m(a)$.

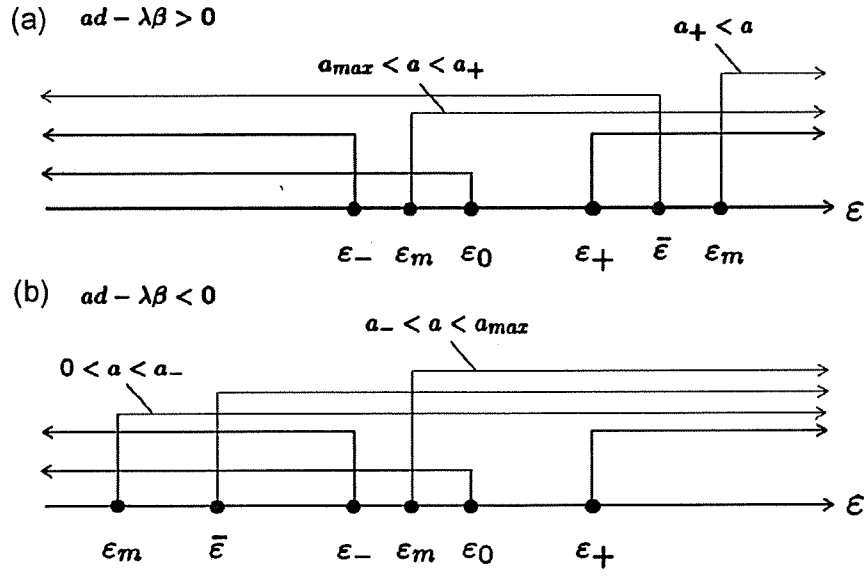

Fig. 8. Graphical presentation of existence conditions for $E_c^{\pm}$ with $h(0)>0$.

Table 2
Existence and stability conditions of the equilibria.

Equilibrium	Existence condition	Stability condition
E_h	Always	$R_0<1$
E_u	$R_0>1$	$\bar{\varepsilon}<\varepsilon$
$(0<a<a_-)$		
E_c^-	$\lambda c/b>\beta$, $\bar{\varepsilon}<\varepsilon<\varepsilon_-$	Always unstable
E_c^+	$\lambda c/b>\beta$, $0\le\varepsilon<\varepsilon_-$	Always stable
$(a_-<a<\bar{a})$		
E_c^+	$\lambda c/b>\beta$, $0\le\varepsilon<\bar{\varepsilon}$	Always stable

$y_c^{\pm}$ are the roots of $g(y)=0$. Therefore, we have $y_c^{\pm 2} = y_c^{\pm}(\lambda c - b\beta - \varepsilon bd)/\varepsilon b\beta - d/\varepsilon\beta$. This leads to

$$\frac{d}{\beta\varepsilon} > y_c^{\pm 2} \iff \frac{2bd}{\lambda c - b\beta - \varepsilon bd} > y_c^{\pm}.$$

$y_c^{\pm}$ can be rewritten as follows:

$$y_c^{\pm} = \frac{2bd}{\lambda c - b\beta - \varepsilon bd \pm \sqrt{(\lambda c - b\beta - \varepsilon bd)^2 - 4\varepsilon b^2 d\beta}},$$

which implies that

$$y_c^+ < \frac{2bd}{\lambda c - b\beta - \varepsilon bd} < y_c^-.$$

Therefore, we can conclude that E_c^- is always unstable if it exists and E_c^+ is always stable if it exists. Consequently, we can summarize the existence and stability conditions in Table 2 ($\bar{\varepsilon}<0$ if $\lambda c - b\beta<0$ and $a_-<\bar{a}$ if $\lambda c - b\beta>0$). We remark that Table 2 includes the case of $\varepsilon = 0$.

References

Altes, H.K., Wodarz, D., Jansen, V.A.A., 2002. The dual role of CD4 T helper cells in the infection dynamics of HIV and their importance for vaccination. J. Theor. Biol. 214, 633–646.

Altes, H.K., Ribeiro, R.M., de Boer, R.J., 2003. The race between initial T-helper expansion and virus growth upon HIV infection influences polyclonality of the response and viral set-point. Proc. R. Soc. London B 270, 1349–1358.

Barber, D.L., Wherry, E.J., Masopust, D., Zhu, B., Allison, J.P., Sharpe, A.H., Freeman, G.J., Ahmed, R., 2006. Restoring function in exhausted CD8 T cells during chronic viral infection. Nature 439, 682–687.

Binley, J.M., Clas, B., Gettie, A., Vesanen, M., Montefiori, D.C., Sawyer, L., Booth, J., Lewis, M., Marx, P.A., Bonhoeffer, S., Moore, J.P., 2000. Passive infusion of immune serum into simian immunodeficiency virus-infected rhesus macaques undergoing a rapid disease course has minimal effect on plasma viremia. Virology 270, 237–249.

Ciupe, M.S., Bivort, B.L., Bortz, D.M., Nelson, P.W., 2006. Estimating kinetic parameters from HIV primary infection data through the eyes of three different mathematical models. Math. Biosci. 200, 1–27.

Cecilia, D., Kleeberger, C., Munoz, A., Giorgi, J.V., Zolla-Pazner, S., 1999. A longitudinal study of neutralizing antibodies and disease progression in HIV-1-infected subjects. J. Infect. Dis. 179, 1365–1374.

Connolly, N.C., Whiteside, T.L., Wilson, C., Kondragunta, V., Rinaldo, C.R., Riddler, S.A., 2008. Therapeutic immunization with human immunodeficiency virus type 1 (HIV-1) peptide-loaded dendritic cells is safe and induces immunogenicity in HIV-1-infected individuals. Clin. Vaccine Immunol. 15, 284–292.

Davenport, M.P., Ribeiro, R.M., Perelson, A.S., 2004. Kinetics of virus-specific CD8+ T cells and the control of human immunodeficiency virus infection. J. Virol. 78, 10096–100103.

De Boer, R.J., Boerlijst, M.C., 1994. Diversity and virulence thresholds in AIDS. Proc. Natl. Acad. Sci. USA 94, 544–548.

Donaghy, H., Pozniak, A., Gazzard, B., Qazi, N., Gilmour, J., Gotch, F., Patterson, S., 2001. Loss of blood CD11c+ myeloid and CD11c− plasmacytoid dendritic cells in patients with HIV-1 infection correlates with HIV-1 RNA virus load. Blood 98, 2574–2576.

Donaghy, H., Gazzard, B., Gotch, F., Patterson, S., 2003. Dysfunction and infection of freshly isolated blood myeloid and plasmacytoid dendritic cells in patients infected with HIV-1. Blood 101, 4505–4511.

Freeman, G.J., Wherry, E.J., Ahmed, R., Sharpe, A.H., 2006. Reinvigorating exhausted HIV-specific T cells via PD-1–PD-1 ligand blockade. J. Exp. Med. 203, 2223–2227.

Galvani, A.P., 2005. The role of mutation accumulation in HIV progression. Proc. R. Soc. London B 272, 1851–1858.

Garcia, F., Lejeune, M., Climent, N., Gil, C., Alcami, J., Morente, V., Alos, L., Ruiz, A., Setoain, J., Fumero, E., Castro, P., Lopez, A., Cruceta, A., Piera, C., Florence, E., Pereira, A., Libois, A., Gonzalez, N., Guila, M., Caballero, M., Lomena, F., Joseph, J., Miro, J.M., Pumarola, T., Plana, M., Gatell, J.M., Gallart, T., 2005. Therapeutic immunization with dendritic cells loaded with heat-inactivated autologous HIV-1 in patients with chronic HIV-1 infection. J. Infect. Dis. 191, 1680–1685.

Hogue, I.B., Bajaria, S.H., Fallert, B.A., Qin, S., Reinhart, T.A., Kirschner, D.E., 2008. The dual role of dendritic cells in the immune response to human immunodeficiency virus type 1 infection. J. Gen. Virol. 89, 2228–2239.

Iwami, S., Nakaoka, S., Takeuchi, Y., 2008. Viral diversity limits immune diversity in asymptomatic phase of HIV infection. Theor. Popul. Biol. 73, 332–341.

Iwami, S., Nakaoka, S., Takeuchi, Y., Immune impairment thresholds in HIV infection, in revision.

Iwasa, Y., Michor, F., Nowak, M.A., 2005. Virus evolution within patients increases pathogenicity. J. Theor. Biol. 232, 17–26.

Janewa, C., Travers, P., Walport, M., Shlomchik, M.J., 2004. Immunobiology: The Immune System in Health and Disease. Garland Pub..

Kawamura, T., Gatanaga, H., Borris, D.L., Connors, M., Mitsuya, H., Blauvelt, A., 2003. Decreased stimulation of CD4+ T cell proliferation and IL-2 production by highly enriched populations of HIV-infected dendritic cells. J. Immunol. 170, 4260–4266.

Kozyrev, I.L., Ibuki, K., Shimada, T., Kuwata, T., Takemura, T., Hayami, M., Miura, T., 2001. Characterization of less pathogenic infectious molecular clones derived from acute-pathogenic SHIV-89.6P stock virus. Virology 282, 6–13.

Lore, K., Sonnerborga, A., Brostrom, C., Goh, L.-E., Perrin, L., McDade, H., Stellbrink, H.-J., Gazzard, B., Weber, R., Napolitano, L.A., vanKooyk, Y., Andersson, J., 2002. Accumulation of DC–SIGN + CD40+ dendritic cells with reduced CD80 and CD86 expression in lymphoid tissue during acute HIV-1 infection. AIDS 16, 683–692.

Mandl, J.N., Regoes, R.R., Garber, D.A., Feinberg, M.B., 2007. Estimating the effectiveness of simian immunodeficiency virus-specific CD8+ T cells from the dynamics of viral immune escape. J. Virol. 81, 11982–11991.

Macatonia, S.E., Lau, R., Patterson, S., Pinching, A.J., Knight, S.C., 1990. Dendritic cell infection, depletion and dysfunction in HIV-infected individuals. Immunology 71, 38–45.

McKnight, A., Clapham, P.R., 1995. Immune escape and tropism of HIV. Trends Microbiol. 3, 356–361.

McMichael, A.J., Rowland-Jones, S.L., 2001. Cellular immune responses to HIV. Nature 410, 980–987.

Meissnera, E.G., Duus, K.M., Gao, F., Yu, X.-F., Su, L., 2004. Characterization of a thymus-tropic HIV-1 isolate from a rapid progressor: role of the envelope. Virology 328, 74–88.

Nowak, M.A., May, R.M., 2000. Virus Dynamics. Oxford University Press, Oxford.

Ogg, G.S., Jin, X., Bonhoeffer, S., Moss, P., Nowak, M.A., Monard, S., Segal, J.P., Cao, Y., Rowland-Jones, S.L., Hurley, A., Markowitz, M., Ho, D.D., McMichael, A.J., Nixon, D.F., 1999. Decay kinetics of human immunodeficiency virus-specific effector cytotoxic T lymphocytes after combination antiretroviral therapy. J. Virol. 73, 797–800.

Patterson, S., English, N.R., Longhurst, H., Balfe, P., Helbert, M., Pinching, A.J., Knight, S.C., 1998. Analysis of human immunodeficiency virus type 1 (HIV-1) variants and levels of infection in dendritic and T cells from symptomatic HIV-1-infected patients. J. Gen. Virol. 79, 247–257.

Perelson, A.S., Neumann, A.U., Markowitz, M., Leonard, J.M., Ho, D.D., 1996. HIV-1 dynamics in vivo: virion clearance rate, infected cell life-span, and viral generation time. Science 271, 1582–1586.

Regoes, R.R., Wodarz, D., Nowak, M.A., 1998. Virus dynamics: the effect of target cell limitation and immune responses on virus evolution. J. Theor. Biol. 191, 451–462.

Richman, D.D., 2001. HIV chemotherapy. Nature 410, 995–1001.

Rinaldo, C.R., 2008. Dendritic cell-based human immunodeficiency virus vaccine. J. Int. Med. 265, 138–158.

Smed-Sorensen, A., Lore, K., Walther-Jallow, L., Anderson, J., Spetz, A., 2004. HIV-1 infected dendritic cells up-regulate cell surface markers but fail to produce IL-12 p70 in response to CD40 ligand stimulation. Blood 104, 2810–2817.

Stafford, M.A., Corey, L., Cao, Y., Daar, E.S., Ho, D.D., Perelson, A.S., 2000. Modeling plasma virus concentration during primary HIV infection. J. Theor. Biol. 203, 285–301.

Thieme, H.R., 2003. Mathematics in Population Biology. Princeton University Press, Princeton.

Tunetsugu-Yokota, Y., 2005. How does HIV infection destroy the host immune system?. J. AIDS Res. 7, 171–179.

Velu, V., Titanji, K., Zhu, B., Husain, S., Pladevega, A., Lai, L., Vanderford, T.H., Chennareddi, L., Silvestri, G., Freeman, G.J., Ahmed, R., Amara, R.R., 2009. Enhancing SIV-specific immunity in vivo by PD-1 blockade. Nature 458, 206–210.

Wu, L., Kewal-Ramani, V.N., 2006. Dendritic-cell interactions with HIV: infection and viral dissemination. Nat. Rev. Immunol. 6, 859–868.

Wodarz, D., Klenerman, P., Nowak, M.A., 1998. Dynamics of cytotoxic T-lymphocyte exhaustion. Proc. R. Soc. London B 265, 191–203.

Wodarz, D., Nowak, M.A., 1999. Specific therapy regimes could engender long-term immunological control of HIV. Proc. Natl. Acad. Sci. USA 96, 14464–14469.

ARTICLE IN PRESS

YVIRO-05592; No. of pages: 10; 4C:

Virology xxx (2010) xxx–xxx

Contents lists available at ScienceDirect

Virology

journal homepage: www.elsevier.com/locate/yviro

In vivo analysis of a new R5 tropic SHIV generated from the highly pathogenic SHIV-KS661, a derivative of SHIV-89.6

Kenta Matsuda, Katsuhisa Inaba, Yoshinori Fukazawa, Megumi Matsuyama, Kentaro Ibuki, Mariko Horiike, Naoki Saito, Masanori Hayami, Tatsuhiko Igarashi, Tomoyuki Miura *

Laboratory of Primate Model, Experimental Research Center for Infectious Diseases, Institute for Virus Research, Kyoto University, 53 Shogoinkawaramachi, Sakyo-ku, Kyoto 606-8507, Japan

ARTICLE INFO

Article history:
Received 9 November 2009
Returned to author for revision
14 December 2009
Accepted 5 January 2010
Available online xxxx

ABSTRACT

Although X4 tropic SHIVs have been studied extensively, they show distinct infection phenotypes from those of R5 tropic viruses, which play an important role in HIV-1 transmission and pathogenesis. To augment the variety of R5 tropic SHIVs, we generated a new R5 tropic SHIV from the highly pathogenic X4 tropic SHIV-KS661, a derivative of SHIV-89.6. Based on consensus amino acid alignment analyses of subtype B R5 tropic HIV-1, five amino acid substitutions in the third variable region successfully changed the secondary receptor preference from X4 to R5. Improvements in viral replication were observed in infected rhesus macaques after two passages, and reisolated virus was designated SHIV-MK38. SHIV-MK38 maintained R5 tropism through *in vivo* passages and showed robust replication in infected monkeys. Our study clearly demonstrates that a minimal number of amino acid substitutions in the V3 region can alter secondary receptor preference and increase the variety of R5 tropic SHIVs.

Introduction

Simian immunodeficiency virus (SIV) macaque models for AIDS have been used extensively to elucidate the pathogenesis of human immunodeficiency virus type 1 (HIV-1) infection. Although SIV is an excellent model virus that has contributed to various virological discoveries, SIV has many limitations as an HIV-1 model. Because the antigenicity of SIV is different from that of HIV-1, it is difficult to evaluate HIV-1 vaccines in animal models by employing SIV as a challenge virus. This is especially true for evaluating the induction of neutralizing antibodies by HIV-1 vaccine candidates (Baba et al., 2000; Dey et al., 2009; Mascola et al., 2000). In addition to CCR5, SIV utilizes secondary receptors such as GPR1, GPR15 (Bob), and STRL-33 (Bonzo), which are scarcely used by HIV-1 (Clapham and McKnight, 2002). Although there have been no reports that have directly demonstrated the significance of these receptors for *in vivo* pathogenesis, possible influences of these minor receptors cannot be denied.

To supplement the limitations of the SIV model, a simian and human immunodeficiency virus (SHIV) macaque model has been generated. SHIVs were constructed by exchanging the envelope gene and other accessory genes of SIV with that of HIV-1 (Shibata et al., 1991). Therefore, SHIVs share the same envelope antigenicity and receptor usage with HIV-1. In early studies of HIV-1, isolated viruses were mostly X4 or dual tropic because they were isolated from AIDS patients using T-cell lines expressing CXCR4. Because envelope genes from X4 or dual tropic viruses were introduced to generate the chimeric virus, most SHIVs utilize CXCR4 as a secondary receptor. X4 tropic viruses infect distinct subsets of lymphocytes and the mode of viral replication during the acute phase of infection is different from that of R5 tropic viruses (Nishimura et al., 2004). During the acute phase of infection, X4 tropic SHIVs rapidly deplete circulating CD4 positive (+) T cells (Reimann et al., 1996; Sadjadpour et al., 2004). Most infected monkeys fail to seroconvert, because rapid depletion of helper T cells typically occurs within 4 weeks of infection. In contrast, R5 tropic viruses do not show such a catastrophic reduction in CD4+ T cells. The phenotypes observed during X4 SHIV infection are rare during actual HIV-1 infection, and it has been suggested that R5 tropic viruses are mainly involved in HIV-1 transmission and pathogenesis (Margolis and Shattock, 2006). Therefore, there is a demand for R5 tropic SHIVs in this field of research.

There are some R5 tropic SHIVs that have already been used in various experiments, including analyses on the efficacy of broadly neutralizing antibodies (Hessell et al., 2009). Due to the paucity of available R5 tropic SHIVs, however, it is difficult to conduct comparative analyses on the efficacy of neutralizing antibodies between different strains of SHIVs. *In vivo* analyses of neutralizing antibodies should be conducted with more than one or even a mixture of several strains of R5 tropic virus to reflect the wide variety of HIV-1

* Corresponding author. Mailing address: Laboratory of Primate Model, Experimental Research Center for Infectious Diseases, Institute for Virus Research, Kyoto University, 53 Shogoinkawaramachi, Sakyo-ku, Kyoto 606-8507, Japan. Fax: +81 75 761 9335.
E-mail address: tmiura@virus.kyoto-u.ac.jp (T. Miura).

0042-6822/$ – see front matter © 2010 Published by Elsevier Inc.
doi:10.1016/j.virol.2010.01.008

Please cite this article as: Matsuda, K., et al., *In vivo* analysis of a new R5 tropic SHIV generated from the highly pathogenic SHIV-KS661, a derivative of SHIV-89.6, Virology (2010), doi:10.1016/j.virol.2010.01.008

envelope genes that are found worldwide. Therefore, our primary aim was to generate a new R5 tropic SHIV, which carries a different *env* from that of other existing R5 SHIVs.

Currently available R5 SHIVs were constructed by introducing the envelope gene and other accessory genes from R5 tropic HIV-1 into the SIV backbone (Humbert et al., 2008; Luciw et al., 1995). There is one report that demonstrated the construction of an R5 tropic SHIV by exchanging the whole third variable region (V3) of an X4 tropic SHIV with that of an R5 SHIV (Ho et al., 2005). This study clearly indicated that the V3 region of the envelope gene determines the secondary receptor preference *in vivo*. Although other studies have indicated that there are specific amino acids within the V3 region that are responsible for receptor preference (Cardozo et al., 2007; Yamaguchi-Kabata et al., 2004), there have been no reports demonstrating the generation of R5 tropic SHIV by the introduction of specific amino acid substitutions to the V3 region. Therefore, our secondary aim in this study was to alter the receptor usage of a well-studied X4 tropic SHIV by introducing a minimal number of amino acid substitutions in the *env* V3 region. The consensus amino acid alignment of subtype B R5 tropic HIV-1, which is strongly correlated with secondary receptor usage (Cardozo et al., 2007; Yamaguchi-Kabata et al., 2004), was introduced to the V3 region of a highly pathogenic SHIV-KS661 that possesses the typical infection phenotype of X4 tropic SHIV (Fukazawa et al., 2008; Miyake et al., 2006). SHIV-KS661 is a molecular clone constructed from the consensus sequence of SHIV-C2/1 (Gen Bank accession number AF21718) (Shinohara et al., 1999), a derivative of the non-pathogenic SHIV-89.6

Results

Generation of R5 tropic SHIV-MK1 from the highly pathogenic X4 tropic SHIV-KS661

The X4 tropic virus SHIV-KS661, a derivative of SHIV-89.6, depletes CD4+ T lymphocytes in systemic tissues within weeks of infection and causes AIDS-like symptoms in macaque monkeys (Fukazawa et al., 2008; Miyake et al., 2006). To convert the virus into an R5 tropic virus, we introduced five amino acid substitutions in the V3 region of SHIV-KS661 by site-directed mutagenesis. The positions of the substitutions were selected using information from alignment of the V3 amino acids of R5 tropic HIV-1 (Cardozo et al., 2007; Yamaguchi-Kabata et al., 2004). All five substitutions (E305K, R306S, R318T, R319G, and N320D) were accompanied by changes in electrical charge. As a result, the net charge of the V3 region shifted towards being more acidic (Fig. 1A). To determine whether this mutant, designated SHIV-MK1, was capable of replication within monkey cells, we spinoculated SHIV-MK1 on rhPBMCs at an MOI of 0.1. The RT activity in the supernatant was monitored daily. The X4 tropic SHIV-DH12R-CL-7 and parental SHIV-KS661 actively replicated on rhPBMCs, reaching its peak RT activity level 4 days after inoculation. The R5 tropic SIVmac239 reached its peak RT value at the same time point; however, the peak value was less than 50% of that of SHIV-DH12R-CL-7 and SHIV-KS661. SHIV-MK1 also replicated on rhPBMCs, but it took 2 days longer to reach peak RT activity levels, and the peak RT value was significantly lower than that of the parental SHIV-KS661 (Fig. 1B).

Next, to determine whether SHIV-MK1 was capable of utilizing CCR5, but not CXCR4, we conducted a small molecule inhibitor assay. Briefly, SIVmac239, SHIV-DH12R-CL-7, SHIV-KS661, or SHIV-MK1 was spinoculated on rhPBMCs that were preincubated with AD101 (R5 inhibitor), AMD3100 (X4 inhibitor), or both inhibitors at various concentrations. The supernatant RT activities were measured 5 days post-inoculation. The replication of X4 tropic SHIV-DH12-CL-7 was inhibited with AMD3100 in a dose-dependent manner; however, it was not restrained with AD101 as described previously (Igarashi et al., 1999, 2003; Sadjapour et al., 2004). The same pattern was observed in SHIV-KS661-infected rhPBMCs, thus indicating that this virus is also an X4 tropic virus. In contrast, there was no replication inhibition of R5 tropic SIVmac239 in the presence of AMD3100; however, dose-dependent inhibition was observed in the presence of AD101. This result is consistent with other reports (Marcon et al., 1997; Zhang et al., 2000). SHIV-MK1 exhibited the same inhibition profile as SIVmac239, indicating that this virus predominantly utilizes CCR5, but not CXCR4, as an entry secondary receptor.

R5 tropic SHIV-MK1 can replicate in rhesus macaques

To determine whether SHIV-MK1 is capable of replication in rhesus macaques, we intravenously inoculated two monkeys (MM482 and MM483) with 20,000 TCID50 SHIV-MK1. Large amount of virus was inoculated to this group of monkey because *in vitro* replication of SHIV-MK1 was significantly weak compared with that of parental SHIV-KS661. As a control, two other monkeys (MM455 and MM459) were infected with 2000 TCID50 SHIV-KS661, a sufficient amount of virus to induce AIDS-like symptoms (Fukazawa et al., 2008; Miyake et al., 2006). Plasma viral RNA loads were monitored periodically using quantitative RT-PCR. Both groups of infected monkeys exhibited viremia, which reached peak plasma viral RNA loads of 10^6–10^8 copies/ml 2 weeks post-infection. In SHIV-KS661-infected monkeys, the set point of plasma viral RNA loads was between 10^4 and 10^6 copies/ml (Fig. 2Ai). In contrast, the plasma viral RNA load in one of the two monkeys infected with SHIV-MK1 was undetectable by 6 weeks post-infection, although 10-fold more virus was inoculated. The other monkey maintained 10^3–10^4 copies/ml plasma viral RNA for more than 25 weeks post-infection (Fig. 2Aii).

Next, circulating CD4+ T lymphocytes were analyzed by fluorescence activated cell sorting (FACS) to elucidate the impact of infection on lymphocyte subsets. As previously reported, X4 tropic SHIV-KS661 caused a massive depletion of circulating CD4+ T lymphocytes within 4 weeks post-infection (Fig. 2Bi). In contrast, circulating CD4+ T lymphocytes transiently decreased in monkeys infected with SHIV-MK1; however, they tended to recover by 24 weeks post-infection (Fig. 2Bii).

Because X4 tropic viruses preferably target naive CD4+ T lymphocytes, and R5 tropic viruses preferably target memory CD4+ T lymphocytes, circulating memory and naive CD4+ T lymphocytes were analyzed. The ratios of memory and naive CD4+ T cells were monitored 0, 2, 4, and 8 weeks post-SHIV-MK1 infection (Fig. 2C). Consistent with previous reports (Nishimura et al., 2004), X4 tropic SHIV-KS661 preferentially depleted naive T lymphocytes by 2 weeks post-infection. Although there was a subtle reduction in CD4+ T lymphocytes, the ratio of memory and naive CD4+ T lymphocytes did not change in SHIV-MK1-infected monkeys. This result indicates that a reduction in CD4+ T cells during SHIV-MK1 infection was not sufficient to alter the ratio of memory T cells, at least in circulating T lymphocytes.

The intestine is an effecter site where most CD4+ T lymphocytes are memory cells, and is the primary target for R5 tropic viruses (Harouse et al., 1999; Veazey et al., 1998). To elucidate the impact of viral infection in the intestine, tissue samples from the jejunum were obtained periodically and CD4+ T lymphocyte subsets were analyzed (Fig. 2D). As reported previously, CD4+ T lymphocytes of KS661-infected monkeys were depleted by 4 weeks post-infection (Fukazawa et al., 2008; Miyake et al., 2006). Although CD4+ T lymphocyte depletion was observed in one of the SHIV-MK1-infected monkeys (MM482) within 4 weeks post-infection, CD4+ T lymphocytes recovered as plasma viral RNA loads decreased. Another SHIV-MK1 infected monkey (MM483) whose plasma viral RNA load dropped below detectable levels showed only a transient reduction in CD4+ lymphocytes 5 weeks after infection. Taken together, these results suggest that, although the magnitude of jejunal CD4+ T-cell reduction was greater than that of circulating CD4+ T cells, the capability of

Please cite this article as: Matsuda, K., et al., *In vivo* analysis of a new R5 tropic SHIV generated from the highly pathogenic SHIV-KS661, a derivative of SHIV-89.6, Virology (2010), doi:10.1016/j.virol.2010.01.008

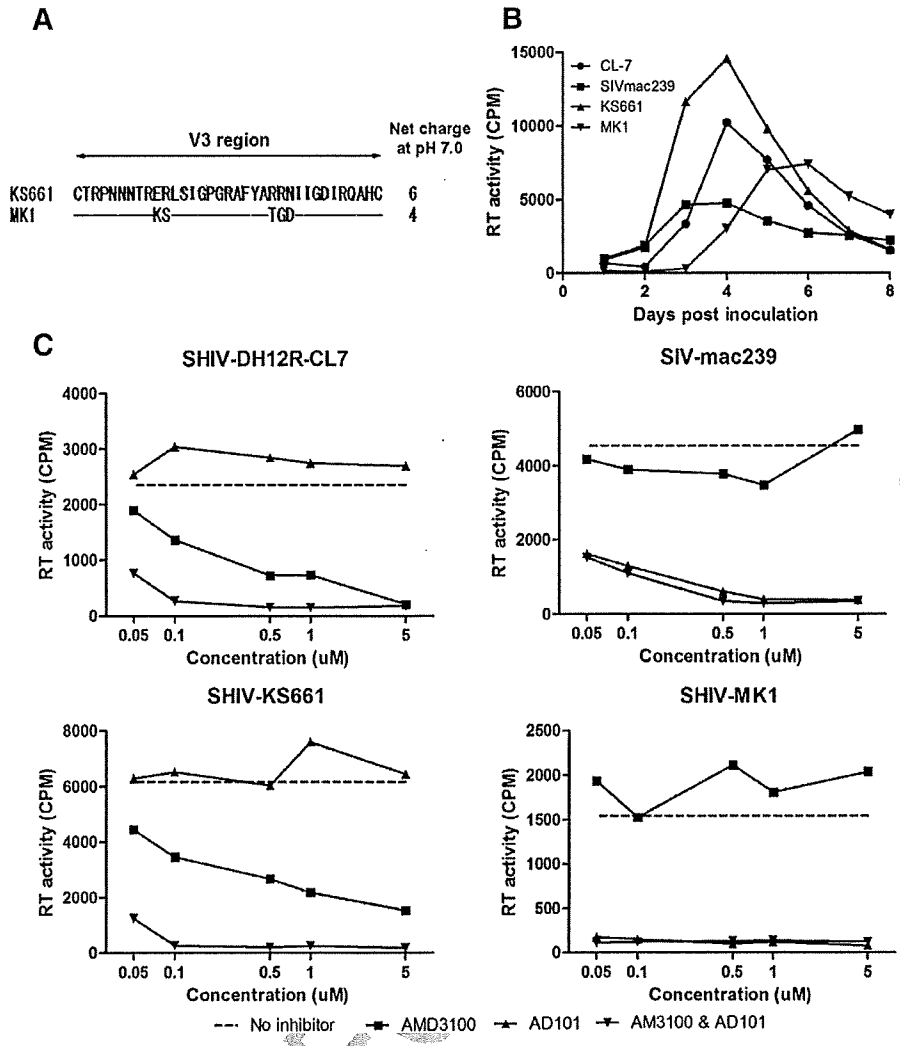

Fig. 1. Construction and *in vitro* analysis of SHIV-MK1. (A) gp120 V3 amino acid alignment of SHIV-MK1. Amino acid substitution positions are indicated under the parental SHIV-KS661 alignment. The net charge at pH 7.0 is indicated beside each amino acid alignment. (B) SHIV and SIV replication in rhPBMCs. The replication of control viruses (SIVmac239, SHIV-DH12R-CL7, and SHIV-KS661) and the mutant virus (SHIV-MK1) are shown. Culture supernatants were collected at the indicated time points, and RT activity was determined. Representative results of three independent experiments are shown. (C) Secondary receptor inhibitor sensitivity of the three SHIV inocula and an SIV control. The inoculum viruses SHIV-DH12R-CL7, SIVmac239, SHIV-KS661, and SHIV-MK1 were spinoculated on rhPBMCs in the presence of the indicated small molecule inhibitors. The inhibitor concentrations used were 0.05, 0.1, 0.5, 1, and 5 μM. The RT activity on day 5 post-infection was determined by the absence (dashed line) or presence of an inhibitor in the medium.

SHIV-MK1 to cause CD4+ T lymphocyte depletion in the jejunum is not as strong as the parental SHIV-KS661.

In vivo passage and characterization of the reisolated virus, SHIV-MK38

To adapt SHIV-MK1, we conducted *in vivo* passages. Briefly, disaggregated lymphocytes from inguinal lymph nodes and fresh blood collected from SHIV-MK1-infected MM482, were mixed and intravenously inoculated into an uninfected monkey, MM498. During the first passage, MM498 showed a plasma viral RNA load peak and set point equal to that of SHIV-MK1-infected MM482. During the second passage, disaggregated lymphocytes from inguinal lymph nodes and fresh blood collected from MM498 were mixed and intravenously inoculated into an uninfected monkey, MM504. MM504 showed a peak plasma viral RNA load of 5×10^7 copies/ml, which is slightly higher than that of MM482 and MM498. Furthermore, the set point of the viral load ranged from 10^4 to 10^6 copies/ml, which is approximately 10 times higher than that of MM482 and MM498 (Fig. 3A).

Although the inoculum doses were different in passaged monkeys, this result suggests that SHIV-MK1 acquired a better replicative capacity through *in vivo* passage. Therefore, we decided to reisolate the virus from MM504 for *in vitro* characterization. Briefly, CD8-depleted PBMCs from MM504 and an uninfected monkey were co-cultured for 2 weeks. The culture supernatant with the highest RT activity was stored in liquid nitrogen. This virus stock was designated SHIV-MK38.

First, we examined the replication kinetics of SHIV-MK38 in rhPBMCs. The infection assay revealed that although SHIV-MK38 could not replicate as fast or as efficiently as the parental KS661, there was a slight improvement in replication capacity compared with the original SHIV-MK1 (Fig. 3B). This result indicates that mutations that arose through *in vivo* passage increased replication ability in rhPBMCs.

As shown in Fig. 1B, however, X4 tropic viruses (SHIV-DH12R-CL-7 and SHIV-KS661) usually show fast and efficient replication in PBMCs compared with that of R5 tropic viruses (SIVmac239 and SHIV-MK1). Hence, there is the possibility of reversion in the V3 region, which may give SHIV-MK38 the appearance of having better replication capacity

Please cite this article as: Matsuda, K., et al., *In vivo* analysis of a new R5 tropic SHIV generated from the highly pathogenic SHIV-KS661, a derivative of SHIV-89.6, Virology (2010), doi:10.1016/j.virol.2010.01.008

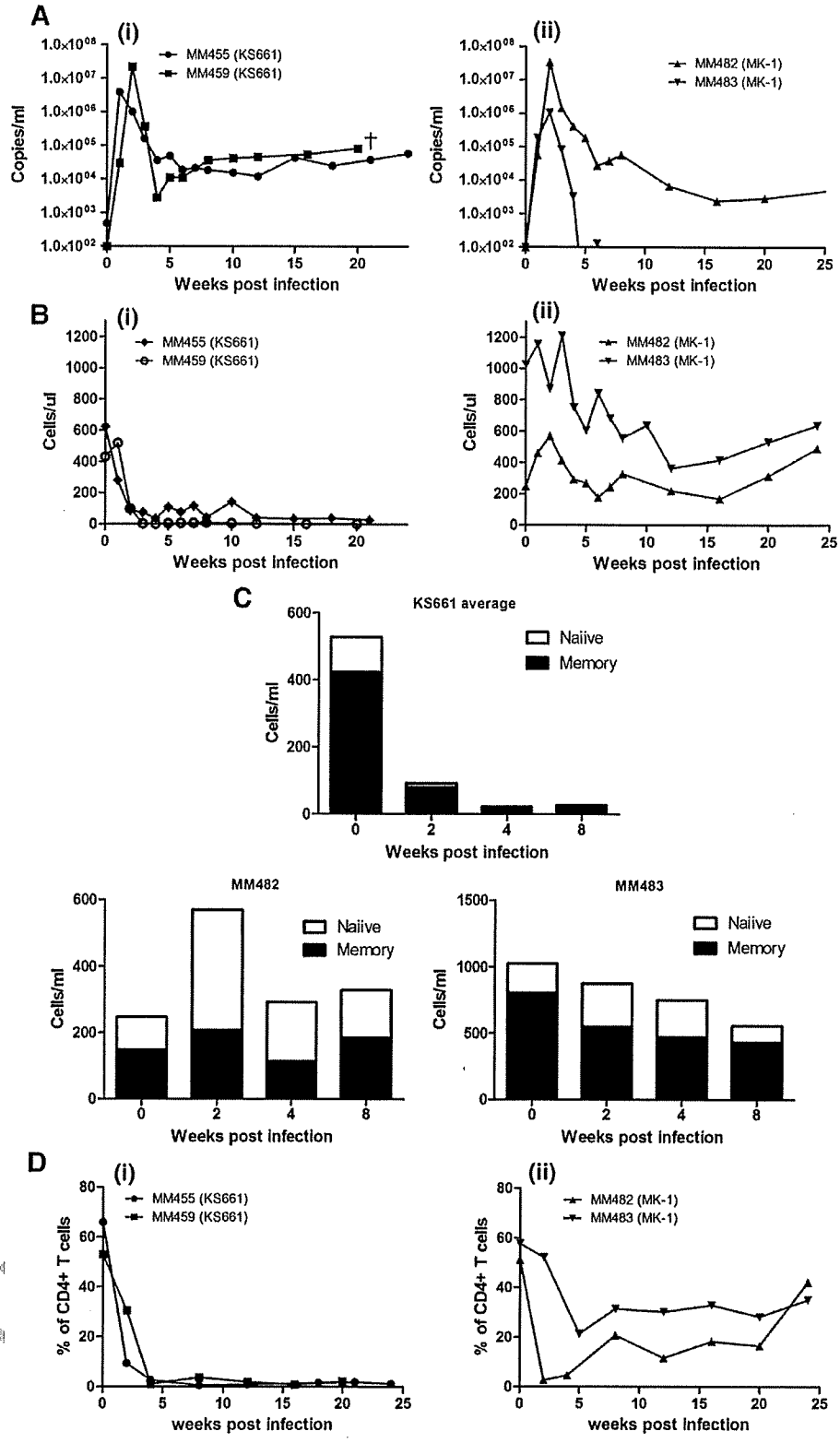

Fig. 2. *In vivo* replication of MK1. (A) Plasma viral RNA loads in SHIV-infected rhesus monkeys were measured at the indicated times. A total of 2000 TCID50 SHIV-KS661 was inoculated intravenously into MM455 and MM459 as a control group (i) and 20,000 TCID50 SHIV-MK1 was inoculated intravenously into MM482 and MM483 (ii). (B) CD4+ T lymphocytes were enumerated using FACS analysis in the SHIV-KS661 infected group (i) and the SHIV-MK1 infected group (ii) over the course of infection. (C) Changes in naive (open bar) and memory (black bar) CD4+ T cells in rhesus macaques inoculated with SHIV-KS661 (average of two infected monkeys) and SHIV-MK1 (MM482 and MM483) 0, 2, 4, and 8 weeks post-inoculation. (D) Percentage of CD4+ T lymphocytes in the jejunum. Tissues from the jejunum were collected from SHIV-KS661 infected monkeys (i) and SHIV-MK1 infected monkeys (ii) with a pediatric enteroscope, and were analyzed by FACS.

Please cite this article as: Matsuda, K., et al., *In vivo* analysis of a new R5 tropic SHIV generated from the highly pathogenic SHIV-KS661, a derivative of SHIV-89.6, Virology (2010), doi:10.1016/j.virol.2010.01.008

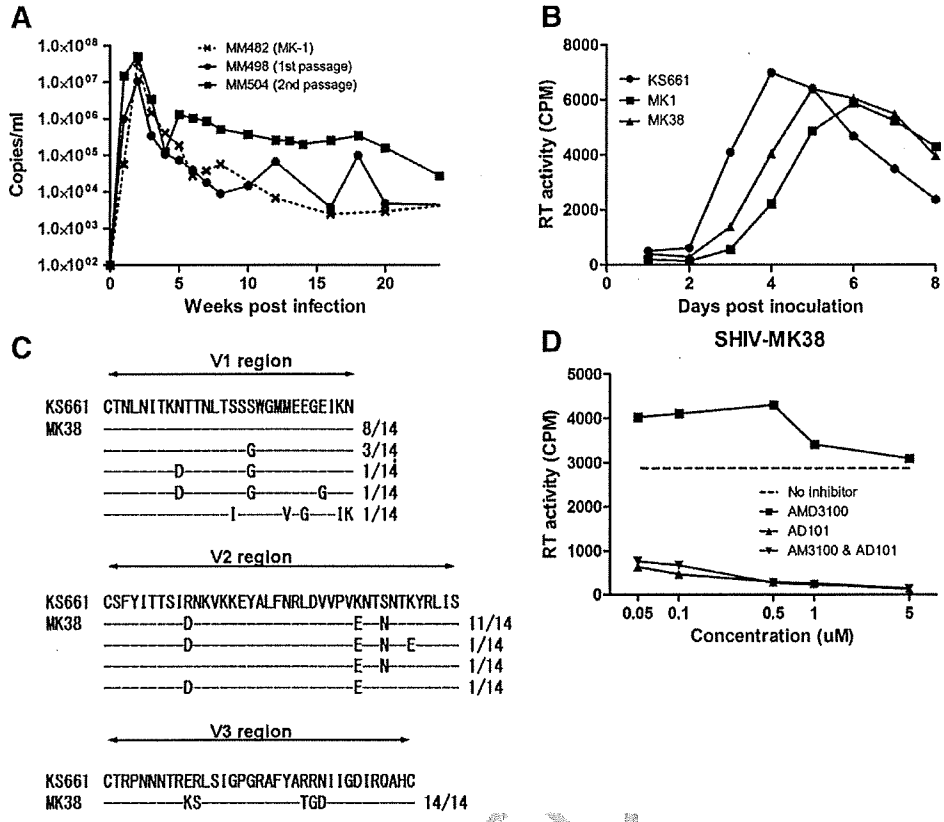

Fig. 3. *In vivo* adaptation of SHIV-MK1, and *in vitro* analysis of reisolated virus. (A) Plasma viral RNA loads of passaged monkeys were measured at the indicated times. The whole blood and dissociated lymph nodes from SHIV-MK1-infected MM482 were transfused into MM498 (first passage) 25 weeks post-inoculation. The whole blood and disaggregated lymph nodes from MM498 were transfused into MM504 (second passage) 5 weeks post-inoculation. (B) SHIV replication in rhPBMCs. The replication of control viruses (SHIV-KS661 and SHIV-MK1) and a passaged virus (SHIV-MK38) is shown. Culture supernatants were collected at the indicated time points, and RT activity was determined. Representative results of three independent experiments are shown. (C) gp120 V1, V2, and V3 amino acid alignment of SHIV-KS661 and 14 clones of SHIV-MK38. The positions of the amino acid substitutions in the 14 clones are indicated under the SHIV-KS661 sequence. (D) Secondary receptor inhibitor sensitivity of the SHIV-MK38 inoculum. RT activity 5 days post-infection was determined in the absence (dashed line) or presence of an inhibitor in the medium.

in rhPBMCs (Cho et al., 1998). Therefore, we examined the viral genome sequence to rule out the presence of reversions in the V3 region. Indeed, there were no back mutations in the V3 region of SHIV-MK38 when the V1 to V3 regions of the *env* sequences from 14 clones were analyzed (Fig. 3C). Nonetheless, we found mutations in the V1 and V2 regions of SHIV-MK38. These mutations have the potential to affect secondary receptor usage.

To confirm whether SHIV-MK38 maintains R5 tropism, we conducted a small molecule inhibitor assay, which revealed that SHIV-MK38 could not replicate in rhPBMCs in the presence of AD101 but could replicate in the presence of AMD3100. This indicates that SHIV-MK38 maintains R5 tropism in the primary cell (Fig. 3D).

In vivo analysis of SHIV-MK38

To evaluate whether SHIV-MK38-infected monkeys show stable infection phenotypes compared with that of SHIV-MK1-infected monkeys, we inoculated three monkeys with 20,000 TCID50 SHIV-MK38. All three infected monkeys possessed a peak plasma viral RNA load of approximately 10^7 copies/ml 12 days after infection. Although the peak plasma viral RNA load was at the same level in these monkeys, set points varied widely (Fig. 4A). That of MM501 was 10^3–10^4 copies/ml, which is similar to that of SHIV-MK1-infected MM482. MM502 had a slightly higher set point of 10^4–10^5 copies/ml, which is similar to that of MM504. Finally, MM481 had the highest set point, at 10^6–10^7 copies/ml. No monkey showed a decrease in viral RNA load under the detectable level, indicating that SHIV-MK38 robustly replicates in rhesus macaques.

Next, reductions in circulating CD4+ T cells were analyzed. Unlike SHIV-MK1 infection, all of the SHIV-MK38-infected monkeys exhibited a continuous reduction in CD4+ T cells without signs of recovery (Fig. 4B). The impact of infection on ratios of circulating memory and naive CD4+ T cells was also analyzed. Compared with monkeys infected with SHIV-MK1, SHIV-MK38 preferentially reduced memory fractions of CD4+ T cells (Figs. 2C and 4C).

To elucidate how improvements in viral replication affect the reduction of CD4+ T cells at effector sites, tissue samples from the jejunum were obtained periodically and CD4+ T lymphocyte subsets were analyzed. In SHIV-MK38-infected monkeys, CD4+ T cells were rapidly reduced by 2 weeks post-infection, as seen in SHIV-MK1 infection. Furthermore, recovery of CD4+ T cells was not observed in infected monkeys. In particular, CD4+ T cells in MM481 were depleted throughout the observation period (Figs. 2D and 4D). These data indicate that SHIV-MK38 has an increased ability to reduce CD4+ T cells and maintain higher plasma viral RNA loads in infected monkeys compared with pre-adapted SHIV-MK1.

Discussion

Based on the analysis of consensus amino acid alignments of subtype B R5 viruses, five amino acid substitutions (E305K, R306S, R318T, R319G, and N320D) were introduced into the V3 region of the pathogenic SHIV-KS661 *env* gene by site-directed mutagenesis. These

Please cite this article as: Matsuda, K., et al., *In vivo* analysis of a new R5 tropic SHIV generated from the highly pathogenic SHIV-KS661, a derivative of SHIV-89.6, Virology (2010), doi:10.1016/j.virol.2010.01.008

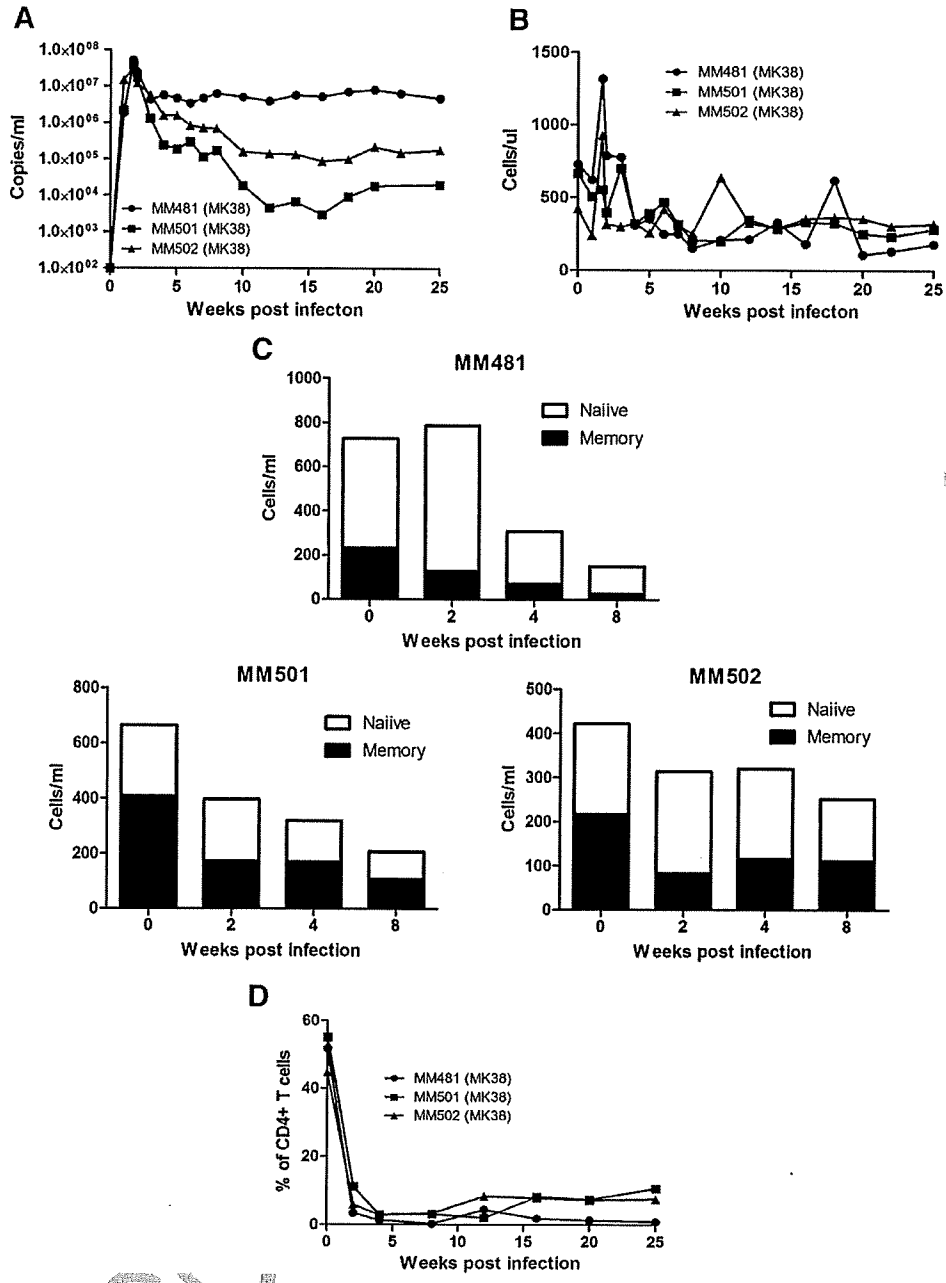

Fig. 4. *In vivo* replication of SHIV-MK38. (A) Plasma viral RNA loads in SHIV-infected rhesus monkeys were measured at the indicated times. A total of 20,000 TCID50 SHIV-MK38 were inoculated into MM481, MM501, and MM502. (B) CD4+ T lymphocytes were enumerated using FACS analysis in SHIV-MK38-infected monkeys over the course of infection. (C) Changes in naïve (open bar) and memory (filled bar) CD4+ T cells in rhesus macaques inoculated with SHIV-MK38 0, 2, 4, and 8 weeks post-inoculation. (D) Percentage of CD4+ T lymphocytes in the jejunum. Tissues from the jejunum were collected from SHIV-MK38-infected monkeys with a pediatric enteroscope, and analyzed by FACS.

substitutions included the 11/24/25th amino acid of the V3 region, which are strongly correlated with secondary receptor usage (Cardozo et al., 2007; Yamaguchi-Kabata et al., 2004). As expected, these substitutions successfully altered the secondary receptor usage of SHIV-KS661 from X4 to R5 tropic. This result clearly demonstrates for the first time that specific V3 amino acid alignment information from HIV-1 can be applied to SHIV to alter secondary receptor usage, at least in the context of the subtype B envelope. The prediction of viral secondary receptor tropism in HIV-1-infected people prior to the prescription of CCR5 antagonists has important economic and practical implications. There are at least six algorithms that predict viral tropism from the V3 sequence; however, the accuracy of these algorithms must be improved (de Mendoza et al., 2008; Dorr et al., 2005; Fätkenheuer et al., 2005; Mefford et al., 2008). For example, the Web PSSM algorithm (Jensen et al., 2003) predicts that SHIV-MK1 exclusively utilizes CCR5, while the Geno2pheno algorithm (Sing et al., 2007) suggests that it may also utilize CXCR4. In this study, we demonstrated that specific amino acids in the V3 region are responsible for secondary receptor usage both *in vitro* and *in vivo*. Accumulation of this type of information will provide important data that can be used to improve predictions and increase the genotype sensitivity of algorithms.

Although minimal numbers of amino acid substitutions were introduced to change secondary receptor usage, SHIV-MK1 showed

Please cite this article as: Matsuda, K., et al., *In vivo* analysis of a new R5 tropic SHIV generated from the highly pathogenic SHIV-KS661, a derivative of SHIV-89.6, Virology (2010), doi:10.1016/j.virol.2010.01.008

relatively inefficient replication compared with that of parental SHIV-KS661, both *in vitro* and *in vivo*. SHIV-MK1 caused measurable levels of viremia in infected monkeys; however, plasma viral RNA levels dropped below detectable levels in one of two infected monkeys 6 weeks after inoculation, despite the fact that enormous amount of virus was inoculated. When evaluating the efficacy of passively administered neutralizing antibodies, or those induced by candidate anti-HIV-1 vaccines, this variability in viral replication is not desirable for the assessment of efficacy, because it is impossible to determine whether the virus was controlled by natural immune responses or by vaccine-induced immune responses. However, an improvement in viral replication was observed in rhPBMCs after *in vivo* passage of SHIV-MK1. This outcome suggests that, as in the case of other existing R5 tropic SHIVs, *in vivo* adaptation is required regardless of the minimal number of amino acid substitutions (Humbert et al., 2008; Tan et al., 1999).

Because various reports have demonstrated the emergence of the X4 tropic virus from the R5 tropic virus after serial passages (Ho et al., 2007; Pastore et al., 2000), there was a concern over the emergence of the X4 tropic virus through two *in vivo* passages. Although there were only five amino acid substitutions, no reversions in any of the substituted amino acids in the V3 region were observed. Some mutations were accompanied by amino acid substitutions in V1 and V2 regions. Previous reports suggest that these two variable regions may influence secondary receptor preference (Cho et al., 1998); however, a small molecule inhibitor assay revealed that SHIV-MK38 maintained R5 tropism after passage. The V1 and V2 regions also play a role in sensitivity against neutralizing antibodies (Laird et al., 2008; Wei et al., 2003). Although further investigations are required, SHIV-MK38 could have developed mutations in the V1 and V2 regions to modify antigenicity in an attempt to evade neutralizing antibodies (Sagar et al., 2006). Indeed, neutralization assay on TZM-BL cells revealed that neutralizing antibody from an MK1-infected monkey can neutralize SHIV-KS661 and SHIV-MK1, but fail to neutralize SHIV-MK38. On the other hand, plasma from the monkey in which SHIV-MK38 was isolated could neutralize all three viruses. Thus, the antigenicity was changed through *in vivo* passages (Supplementary Figure). Taken together, these results suggest that the improved replication of SHIV-MK38 over MK1 was not due to the re-emergence of X4 tropic viruses. Furthermore, the acquisition of mutations outside the V3 region is most likely attributable to the improved replication of SHIV-MK38 *in vivo*.

To confirm the replication advantage of SHIV-MK38 over SHIV-MK1, SHIV-MK38 was intravenously inoculated into three uninfected monkeys. Despite the fact that the same amount of SHIV-MK38 was inoculated, higher peaks and set points of plasma RNA loads were observed in SHIV-MK38 compared with SHIV-MK1 infection. Although SHIV-MK38-infected monkeys showed no obvious signs of AIDS-like symptoms during the observation period, none of these monkeys was able to control viral replication. A greater reduction in the memory portion of circulating CD4+ T cells was observed in SHIV-MK38-infected monkeys. This preferential reduction of circulating memory CD4+ T cells was well defined in MM481, which correlates with the maintenance of high plasma viral RNA loads throughout the observation period. Reductions of CD4+ T cells in the jejunum of SHIV-MK38-infected monkeys were greater than that of SHIV-MK1-infected monkeys, and there was no obvious recovery during the observation period. These infection phenotypes are characteristic of an R5 tropic virus, which is distinct from the infection of X4 tropic SHIVs such as parental SHIV-KS661 (Fukazawa et al., 2008; Miyake et al., 2006).

Harous et al. clearly demonstrated that R5 tropic virus preferentially reduces mucosal CD4+ T cells where memory CD4+ T cells are abundant, whereas X4 tropic virus preferentially reduces peripheral CD4+ T cells where naive CD4+ T cells are abundant (Harouse et al., 1999). From this observation, it is clear that the receptor preference has strong impact on tissue specific CD4+ T-cell reductions. However, in some cases, systemic and irreversible reduction of CD4+ T cells was observed in highly pathogenic X4 SHIV infection (Fukazawa et al., 2008; Nishimura et al., 2004). It has been suggested that highly pathogenic X4 SHIV preferentially targets naive CD4+ T cells but eventually reduces memory CD4+ T cells (Nishimura et al., 2004). The depletion of CD4+ T cells at the effector site in SHIV-KS661 infected monkeys supports this suggestion (Fig. 2D).

The envelope gene of SHIV-MK38 belongs to subtype B, which can be compared with other subtype B or C R5 tropic SHIVs (Humbert et al., 2008; Tan et al., 1999). Comparing the efficacy of passively administered neutralizing antibodies and their induction by candidate HIV-1 vaccines against a variety of R5 tropic SHIVs would provide a more precise evaluation against a variety of HIV-1 strains worldwide (Wei et al., 2003). Furthermore, despite the fact that SHIV-MK38 is derived from SHIV-KS661, and mutations were obtained through the alteration of secondary receptor usage and passage, SHIV-MK38 is still genetically homologous to SHIV-89.6P, because they both originate from the same molecular clone, SHIV-89.6. Highly pathogenic X4 tropic SHIV-89.6P has been used extensively in various experiments, including vaccine concept evaluations (Shiver et al., 2002). There are claims, however, that the utilization of X4 tropic SHIVs as challenge viruses has led to overestimation of vector-based vaccines (Feinberg and Moore, 2002). Therefore, SHIV-MK38 can be useful in the future to determine whether such overestimations are truly caused by using X4 SHIVs or are due to using an SHIV derived from the specific lineage of SHIV-89.6.

Based on our observations, it can be concluded that R5 tropic SHIV-MK38 can robustly replicate, and we successfully generated a new R5 tropic SHIV by a new method. Although infected monkeys showed no signs of AIDS-like symptoms during the observation period, and further characterization such as neutralization profiles must be conducted, SHIV-MK38 has the potential to be a new R5 SHIV model.

Materials and methods

Virus production

Non-synonymous nucleotide substitutions in the V3 domain of the SHIV-KS661 *env* gene were introduced by site-directed mutagenesis for substitution of amino acids. A 5.9 kb DNA fragment containing the *env* V3 domain was subcloned into a pUC119 vector following digestion with restriction enzymes Sse8387I and XhoI. The resulting vector was designated pKS661v3, and was used as the template for two sets of polymerase chain reaction (PCR). All amplifications were performed as follows: one cycle of denaturation (98 °C, 5 min), 32 cycles of amplification (98 °C, 10 s/60 °C, 30 s/72 °C, 2 min), and an additional cycle for final extension (72 °C, 10 min) using iProof High-Fidelity Master Mix (Bio-Rad Laboratories, Hercules, CA). The following primers were used for the first set of PCR: 5′ CAATACAAGAAAAAGTTTATCTATAGGACCAGGGAGAGCATTTTATGCAACAGGAGACATAATAGGAG 3′ (forward primer corresponding to the 7250–7317th nucleotides of SHIV-KS661; positions of mismatches are underlined) and 5′ GCTGAAGAGGCACAGGCTCCGC 3′ (reverse primer corresponding to the 8633–8612th nucleotide of SHIV-KS661; no mismatches). The following primers were used for the second set of PCR: 5′ CTCCTATTATGTCTCCTGTTGCATAAAATGCTCTCCCTGGTCCTATAGATAAACTTTTCTTGTATTG 3′ (reverse primer corresponding to the 7317–7250th nucleotide of SHIV-KS661; positions of mismatches are underlined) and 5′ CTCCAGGACTAGCATAAATGG 3′ (forward primer corresponding to the 5617–5637th nucleotide of SHIV-KS661; no mismatches). The products from these two sets of PCR were mixed, and overlap PCR was performed using primers 5′ GCTGAAGAGGCACAGGCTCCGC 3′ and 5′ CTCCAGGACTAGCATAAATGG 3′. The PCR product was then digested with the restriction enzymes BsaBI and NcoI. The resulting fragment was introduced back into the pKS661v3

Please cite this article as: Matsuda, K., et al., *In vivo* analysis of a new R5 tropic SHIV generated from the highly pathogenic SHIV-KS661, a derivative of SHIV-89.6, Virology (2010), doi:10.1016/j.virol.2010.01.008

vector, and designated pKS661v3m. Then pKS661v3m DNA with mutations was digested by Sse8387I and XhoI, and the fragment was introduced back into the KS661 full genome plasmid, and designated pMK1.

SHIV-MK1 was prepared by transfecting pMK1 into the 293T cell line using the FuGENE 6 Transfection Reagent (Roche Diagnostics, Indianapolis, IN) and the culture supernatant 48 h after transfection, and was stored in liquid nitrogen until use. The same procedures were conducted to prepare SIVmac239 (Kestler et al., 1991), SHIV-KS661 (Shinohara et al., 1999), and SHIV-DH12R-CL7 (Igarashi et al., 1999). The 50% tissue culture infectious dose (TCID50) was measured using the C8166-CCR5 cell line (Shimizu et al., 2006).

Viral replication on rhPBMCs

Rhesus macaque PBMCs (rhPBMCs), prepared from an uninfected monkey, were suspended in Rosewell Park Memorial Institute (RPMI) 1640 medium supplemented with 10% (vol/vol) fetal bovine serum (FBS), 2 mM L-glutamine, and 1 mM sodium pyruvate, and then stimulated for 20 h with 25 μg/ml Concanavalin A (Sigma-Aldrich, St. Louis, USA), followed by an additional 2-day cultivation with 100 units/ml IL-2 (Shionogi, Osaka, Japan). On day 3, 5×10^4 cells were dispensed into 96-well round-bottom plates in triplicate. The cells were then inoculated with virus at a multiplicity of infection (MOI) of 0.1 using the spinoculation method (O'Doherty et al., 2000). Virion-associated reverse transcriptase (RT) activity of the culture supernatant was monitored periodically (Willey et al., 1988).

Inhibition of viral replication by a small molecule inhibitor

A small molecule inhibitor assay was conducted as described previously (Igarashi et al., 2003), with minor modifications. Briefly, uninfected rhesus PBMCs were prepared as described above. On day 3, 5×10^4 cells were dispensed into 96-well round-bottom plates. Various concentrations (0, 0.05, 0.1, 0.5, 1, and 5 μM) of a small molecule CCR5-specific receptor antagonist (AD101 was provided by Dr. Julie Strizki, Schering Plough Research Institute, Kenilworth, NJ) (Trkola et al., 2002) and/or a CXCR4-specific receptor antagonist (AMD3100; Sigma-Aldrich, St. Louis, MO) (Donzella et al., 1998) were added to duplicate wells and incubated for 1 h at 37 °C. Then each test virus was spinoculated at $1200\times g$ for 1 h at an MOI of 0.1. On day 5 post-infection, virus replications were assessed by RT assay of the culture supernatants.

Virus inoculation

Indian-origin rhesus macaques were used in accordance with the institutional regulations approved by the Committee for Experimental Use of Nonhuman Primates of the Institute for Virus Research, Kyoto University, Kyoto, Japan. Monkeys were housed in a biosafety level 3 facility and all procedures were performed in this facility. Collection of blood, biopsies, and i.v. virus inoculations (2000 TCID50 of SHIV-KS661, 20000 TCID50 of SHIV-MK1, 20000 TCID50 of SHIV-MK38) were performed on monkeys under anesthetization with ketamine hydrochloride (Daiichi-Sankyo, Tokyo, Japan). Plasma viral RNA loads were determined by quantitative RT-PCR as described previously (Kozyrev et al., 2002). Plasma viral RNA loads under 100 copies/ml were characterized as undetectable levels.

Jejunal biopsy

Tissue samples from the jejunum were collected with a pediatric enteroscope (Olympus GIF type XP260N, Olympus Medical System Corp., Tokyo, Japan). Five pieces (samples) of fresh jejunal tissue were placed on a shaker for 2 h at room temperature in 40 ml RPMI 1640 medium containing 10% FBS and 0.01 g collagenase from *Clostridium histolyticum* (Sigma-Aldrich, St. Louis, MO). Disaggregated cells were filtered through glass wool loaded in a 20 ml disposable syringe. Cells were prepared from the filtrate by centrifugation at a speed of 1200 rpm for 10 min. Subsets of lymphocytes in the resuspended cells were analyzed by flow cytometry.

Flow cytometry

To analyze CD4+ T lymphocytes, whole blood and jejunal samples were stained with two fluorescently labeled mouse monoclonal antibodies, fluorescein isothiocyanate (FITC) conjugated anti-monkey CD3 (Clone FN-18, BioSource Intl, Camarillo, CA) and phycoerythrin (PE) conjugated anti-human CD4 (Clone Nu-TH/I; Nichirei, Tokyo, Japan). To analyze memory and naive CD4+ T lymphocytes, whole blood and jejunal samples were stained with three fluorescently labeled mouse monoclonal antibodies, FITC conjugated anti-human CD95 (Clone DX2; BD Pharmingen, Tokyo, Japan), PE conjugated anti-human CD28 (Clone CD28.2; Coulter Immunotech, Marseille, France), and allophycocyanin (APC) conjugated anti-human CD4 (Clone L200; BD Pharmingen). After hemolysis of whole blood and jejunal samples using a lysing solution (Beckton Dickinson, Franklin Lakes, NJ), each type of labeled lymphocyte was examined on a FACScalibur analyzer using Cellquest (BD Biosciences, San Jose, CA). CD95+CD4^{high}+ cells were considered memory T lymphocytes, and CD95-CD28+CD4^{high}+ cells were considered naive T lymphocytes (Pitcher et al., 2002). The absolute number of lymphocytes in the blood was determined using an automated blood counter, KX-21 (Sysmex, Kobe, Japan).

In vivo passage

Inguinal lymph nodes were aseptically collected from MM482 25 weeks after infection. The lymph nodes were minced with scissors, disaggregated using an 85-ml Bellco Tissue Sieve Kit (Bellco Glass, Inc., Vineland, NJ), and filtered through a 100-μm pore cell strainer (REF 35-2360, BD Falcon, Franklin Lakes, NJ). Filtrates were centrifuged and then washed four times with phosphate-buffered saline (PBS). These disaggregated cells were mixed with 2 ml frozen plasma (collected from the animal 8 weeks post-infection and stored at −80 °C) and 20 ml fresh blood from MM482, and then transfused into an uninfected monkey (MM498) intravenously. During the second passage, inguinal lymph nodes were aseptically collected from MM498 5 weeks after infection. The disaggregated inguinal lymph node was mixed with 2 ml frozen plasma (collected 2 weeks post-infection), 5×10^7 cells inguinal lymphocytes (collected 16 days post-infection and stored at −80 °C), and 15 ml fresh blood, and then transfused into an uninfected monkey (MM504).

Reisolation of virus

Fresh blood was obtained from the uninfected monkey, and PBMCs were isolated. These cells were incubated for 30 min with PE labeled anti-CD8 antibody (SK1 clone, BD Pharmingen), then washed once with PBS. Next, cells were incubated with anti-PE MACS beads (Miltenyi Biotec, Bergisch Gladbach, Germany), and CD8− cells were negatively selected with a magnetic column. CD8− PBMCs were cultured as described above.

On day 0, fresh blood was obtained from MM504 (16 weeks post-infection) and CD8 cells were depleted as described above. CD8+ cells were also depleted from frozen PBMCs (obtained from MM504 8 weeks post-infection and stored at −80 °C). These CD8− PBMCs from uninfected and infected monkeys were co-cultured in PBMC culture medium (described above) at a concentration of 2×10^6 cells/ml at 37 °C. Medium was replaced daily for 16 days and culture supernatants were stored at −80 °C. The culture supernatant with the highest RT value was stored in liquid nitrogen. This virus stock was designated SHIV-MK38.

Please cite this article as: Matsuda, K., et al., *In vivo* analysis of a new R5 tropic SHIV generated from the highly pathogenic SHIV-KS661, a derivative of SHIV-89.6, Virology (2010), doi:10.1016/j.virol.2010.01.008

Sequence of V1, V2, and V3 regions of SHIV-MK38

SHIV-MK38 viral stock was used as a template for RT-PCR to amplify the V1 to V3 regions of the *env* gene. The forward primer 5′ GTGTAAAATTAACCCCACTCTGTG 3′ and reverse primer 5′ TGGGAGGGGCATACATTGCTTTTCC 3′ were used for RT-PCR. The amplified DNA fragment was cloned into the pCR2.1 vector using a TA Cloning Kit (Invitrogen, Carlsbad, CA), and 14 clones were sequenced.

Acknowledgments

We thank Dr. Julie Strizki, Schering Plough Research Institute, for providing AD101. This work was supported, in part, by Research on Human Immunodeficiency Virus/AIDS in Health and Labor Sciences research grants from the Ministry of Health, Labor and Welfare, Japan, a grant-in-aid for scientific research from the Ministry of Education and Science, Japan, a research grant for health sciences focusing on drug innovation for AIDS from the Japan Health Sciences Foundation, and a grant from the Program for the Promotion of Fundamental Studies in Health Sciences of the National Institute of Biomedical Innovation (NIBIO) of Japan. The English in this document has been checked by at least two professional editors, both native speakers of English. For a certificate, see: http://www.textcheck.com/certificate/fMOCEU.

Appendix A. Supplementary data

Supplementary data associated with this article can be found, in the online version, at doi:10.1016/j.virol.2010.01.008.

References

Baba, T.W., Liska, V., Hofmann-Lehmann, R., Vlasak, J., Xu, W., Ayehunie, S., Cavacini, L.A., Posner, M.R., Katinger, H., Stiegler, G., Bernacky, B.J., Rizvi, T.A., Schmidt, R., Hill, L.R., Keeling, M.E., Lu, Y., Wright, J.E., Chou, T.C., Ruprecht, R.M., 2000. Human neutralizing monoclonal antibodies of the IgG1 subtype protect against mucosal simian–human immunodeficiency virus infection. Nat. Med. 6 (2), 200–206.

Cardozo, T., Kimura, T., Philpott, S., Weiser, B., Burger, H., Zolla-Pazner, S., 2007. Structural basis for coreceptor selectivity by the HIV type 1 V3 loop. AIDS Res. Hum. Retroviruses 23 (3), 415–426.

Cho, M.W., Lee, M.K., Carney, M.C., Berson, J.F., Doms, R.W., Martin, M.A., 1998. Identification of determinants on a dualtropic human immunodeficiency virus type 1 envelope glycoprotein that confer usage of CXCR4. J. Virol. 72 (3), 2509–2515.

Clapham, P.R., McKnight, A., 2002. Cell surface receptors, virus entry and tropism of primate lentiviruses. J. Gen. Virol. 83 (Pt 8), 1809–1829.

de Mendoza, C., Van Baelen, K., Poveda, E., Rondelez, E., Zahonero, N., Stuyver, L., Garrido, C., Villacian, J., Soriano, V., Spanish HIV Seroconverter Study Group, 2008. Performance of a population-based HIV-1 tropism phenotypic assay and correlation with V3 genotypic prediction tools in recent HIV-1 seroconverters. J. Acquir. Immune. Defic. Syndr. 48 (3), 241–244.

Dey, B., Svehla, K., Xu, L., Wycuff, D., Zhou, T., Voss, G., Phogat, A., Chakrabarti, B.K., Li, Y., Shaw, G., Kwong, P.D., Nabel, G.J., Mascola, J.R., Wyatt, R.T., 2009. Structure-based stabilization of HIV-1 gp120 enhances humoral immune responses to the induced co-receptor binding site. PLoS Pathog. 5 (5), e1000445.

Donzella, G.A., Schols, D., Lin, S.W., Este, J.A., Nagashima, K.A., Maddon, P.J., Allaway, G.P., Sakmar, T.P., Henson, G., De Clercq, E., Moore, J.P., 1998. AMD3100, a small molecule inhibitor of HIV-1 entry via the CXCR4 co-receptor. Nat. Med. 4, 72–77.

Dorr, P., Westby, M., Dobbs, S., Griffin, P., Irvine, B., Macartney, M., Mori, J., Rickett, G., Smith-Burchnell, C., Napier, C., Webster, R., Armour, D., Price, D., Stammen, B., Wood, A., Perros, M., 2005. Maraviroc (UK-427,857), a potent, orally bioavailable, and selective small-molecule inhibitor of chemokine receptor CCR5 with broad-spectrum anti-human immunodeficiency virus type 1 activity. Antimicrob. Agents. Chemother. 49 (11), 4721–4732.

Fätkenheuer, G., Pozniak, A.L., Johnson, M.A., Plettenberg, A., Staszewski, S., Hoepelman, A.I., Saag, M.S., Goebel, F.D., Rockstroh, J.K., Dezube, B.J., Jenkins, T.M., Medhurst, C., Sullivan, J.F., Ridgway, C., Abel, S., James, I.T., Youle, M., van der Ryst, E., 2005. Efficacy of short-term monotherapy with maraviroc, a new CCR5 antagonist, in patients infected with HIV-1. Nat. Med. 11 (11), 1170–1172 Epub 2005 Oct 5.

Feinberg, M.B., Moore, J.P., 2002. AIDS vaccine models: challenging challenge viruses. Nat. Med 8 (3), 207–210.

Fukazawa, Y., Miyake, A., Ibuki, K., Inaba, K., Saito, N., Motohara, M., Horiuchi, R., Himeno, A., Matsuda, K., Matsuyama, M., Takahashi, H., Hayami, M., Igarashi, T., Miura, T., 2008. Small intestine CD4+ T cells are profoundly depleted during acute simian–human immunodeficiency virus infection, regardless of viral pathogenicity. J. Virol. 82 (12), 6039–6044 Electronic publication 2008 Apr 9.

Harouse, J.M., Gettie, A., Tan, R.C., Blanchard, J., Cheng-Mayer, C., 1999. Distinct pathogenic sequela in rhesus macaques infected with CCR5 or CXCR4 utilizing SHIVs. Science 30 (284(5415)), 816–819.

Hessell, A.J., Rakasz, E.G., Poignard, P., Hangartner, L., Landucci, G., Forthal, D.N., Koff, W. C., Watkins, D.I., Burton, D.R., 2009. Broadly neutralizing human anti-HIV antibody 2G12 is effective in protection against mucosal SHIV challenge even at low serum neutralizing titers. PLoS Pathog. 5 (5), e1000433.

Ho, S.H., Shek, L., Gettie, A., Blanchard, J., Cheng-Mayer, C., 2005. V3 loop-determined coreceptor preference dictates the dynamics of CD4+-T-cell loss in simian–human immunodeficiency virus-infected macaques. J. Virol. 79 (19), 12296–12303.

Ho, S.H., Tasca, S., Shek, L., Li, A., Gettie, A., Blanchard, J., Boden, D., Cheng-Mayer, C., 2007. Coreceptor switch in R5-tropic simian/human immunodeficiency virus-infected macaques. J. Virol. 81 (16), 8621–8633.

Humbert, M., Rasmussen, R.A., Song, R., Ong, H., Sharma, P., Chenine, A.L., Kramer, V.G., Siddappa, N.B., Xu, W., Else, J.G., Novembre, F.J., Strobert, E., O'Neil, S.P., Ruprecht, R.M., 2008. SHIV-1157i and passaged progeny viruses encoding R5 HIV-1 clade C env cause AIDS in rhesus monkeys. Retrovirology 17 (5), 94.

Igarashi, T., Endo, Y., Englund, G., Sadjadpour, R., Matano, T., Buckler, C., Buckler-White, A., Plishka, R., Theodore, T., Shibata, R., Martin, M., 1999. Emergence of a highly pathogenic simian/human immunodeficiency virus in a rhesus macaque treated with anti-CD8 mAb during a primary infection with a nonpathogenic virus. Proc. Natl. Acad. Sci. U. S. A. 96 (24), 14049–14054.

Igarashi, T., Donau, O.K., Imamichi, H., Dumaurier, M.J., Sadjadpour, R., Plishka, R.J., Buckler-White, A., Buckler, C., Suffredini, A.F., Lane, H.C., Moore, J.P., Martin, M.A., 2003. Macrophage-tropic simian/human immunodeficiency virus chimeras use CXCR4, not CCR5, for infections of rhesus macaque peripheral blood mononuclear cells and alveolar macrophages. J. Virol. 77 (24), 13042–13052.

Kozyrev, I.L., Miura, T., Takemura, T., Kuwata, T., Ui, M., Ibuki, K., Iida, T., Hayami, M., 2002. Co-expression of interleukin-5 influences replication of simian/human immunodeficiency viruses in vivo. J. Gen. Virol. 83, 1183–1188.

Jensen, M.A., Li, F.S., van 't Wout, A.B., Nickle, D.C., Shriner, D., He, H.X., McLaughlin, S., Shankarappa, R., Margolick, J.B., Mullins, J.I., 2003. Improved coreceptor usage prediction and genotypic monitoring of R5-to-X4 transition by motif analysis of human immunodeficiency virus type 1 env V3 loop sequences. J. Virol. 77 (24), 13376–13388.

Kestler III, H.W., Ringler, D.J., Mori, K., Panicali, D.L., Sehgal, P.K., Daniel, M.D., Desrosiers, R.C., 1991. Importance of the nef gene for maintenance of high virus loads and for development of AIDS. Cell 65 (4), 651–662.

Laird, M.E., Igarashi, T., Martin, M.A., Desrosiers, R.C., 2008. Importance of the V1/V2 loop region of simian–human immunodeficiency virus envelope glycoprotein gp120 in determining the strain specificity of the neutralizing antibody response. J. Virol. 82 (22), 11054–11065.

Li, M., Gao, F., Mascola, J.R., Stamatatos, L., Polonis, V.R., Koutsoukos, M., Voss, G., Goepfert, P., Gilbert, P., Greene, K.M., Bilska, M., Kothe, D.L., Salazar-Gonzalez, J.F., Wei, X., Decker, J.M., Hahn, B.H., Montefiori, D.C., 2005. Human immunodeficiency virus type 1 env clones from acute and early subtype B infections for standardized assessments of vaccine-elicited neutralizing antibodies. J. Virol. 79 (16), 10108–10125.

Luciw, P.A., Pratt-Lowe, E., Shaw, K.E., Levy, J.A., Cheng-Mayer, C., 1995. Persistent infection of rhesus macaques with T-cell-line-tropic and macrophage-tropic clones of simian/human immunodeficiency viruses (SHIV). Proc. Natl. Acad. Sci. U. S. A. 92 (16), 7490–7494.

Marcon, L., Choe, H., Martin, K.A., Farzan, M., Ponath, P.D., Wu, L., Newman, W., Gerard, N., Gerard, C., Sodroski, J., 1997. Utilization of C-C chemokine receptor 5 by the envelope glycoproteins of a pathogenic simian immunodeficiency virus, SIV-mac239. J. Virol. 71 (3), 2522–2527.

Margolis, L., Shattock, R., 2006. Selective transmission of CCR5-utilizing HIV-1: the 'gatekeeper' problem resolved? Nat. Rev. Microbiol. 4 (4), 312–317.

Mascola, J.R., Stiegler, G., VanCott, T.C., Katinger, H., Carpenter, C.B., Hanson, C.E., Beary, H., Hayes, D., Frankel, S.S., Birx, D.L., Lewis, M.G., 2000. Protection of macaques against vaginal transmission of a pathogenic HIV-1/SIV chimeric virus by passive infusion of neutralizing antibodies. Nat. Med. 6 (2), 207–210.

Mefford, M.E., Gorry, P.R., Kunstman, K., Wolinsky, S.M., Gabuzda, D., 2008. Bioinformatic prediction programs underestimate the frequency of CXCR4 usage by R5X4 HIV type 1 in brain and other tissues. AIDS Res. Hum. Retroviruses 24 (9), 1215–1220.

Miyake, A., Ibuki, K., Enose, Y., Suzuki, H., Horiuchi, R., Motohara, M., Saito, N., Nakasone, T., Honda, M., Watanabe, T., Miura, T., Hayami, M., 2006. Rapid dissemination of a pathogenic simian/human immunodeficiency virus to systemic organs and active replication in lymphoid tissues following intrarectal infection. J. Gen. Virol. 87, 1311–1320.

Nishimura, Y., Igarashi, T., Donau, O.K., Buckler-White, A., Buckler, C., Lafont, B.A., Goeken, R.M., Goldstein, S., Hirsch, V.M., Martin, M.A., 2004. Highly pathogenic SHIVs and SIVs target different CD4+ T cell subsets in rhesus monkeys, explaining their divergent clinical courses. Proc. Natl. Acad. Sci. U. S. A. 101 (33), 12324–12329.

O'Doherty, U., Swiggard, W.J., Malim, M.H., 2000. Human immunodeficiency virus type 1 spinoculation enhances infection through virus binding. J. Virol. 74, 10074–10080.

Pastore, C., Ramos, A., Mosier, D.E., 2000. Intrinsic obstacles to human immunodeficiency virus type 1 coreceptor switching. J. Virol. 74 (15), 6769–6776.

Pitcher, C.J., Hagen, S.I., Walker, J.M., Lum, R., Mitchell, B.L., Maino, V.C., Axthelm, M.K., Picker, L.J., 2002. Development and homeostasis of T cell memory in rhesus macaque. J. Immunol. 168 (1), 29–43.

Reimann, K.A., Li, J.T., Veazey, R., Halloran, M., Park, I.W., Karlsson, G.B., Sodroski, J., Letvin, N.L., 1996. A chimeric simian/human immunodeficiency virus expressing a primary patient human immunodeficiency virus type 1 isolate env causes an AIDS-like disease after in vivo passage in rhesus monkeys. J. Virol. 70 (10), 6922–6928.

Please cite this article as: Matsuda, K., et al., *In vivo* analysis of a new R5 tropic SHIV generated from the highly pathogenic SHIV-KS661, a derivative of SHIV-89.6, Virology (2010), doi:10.1016/j.virol.2010.01.008

Sadjadpour, R., Theodore, T.S., Igarashi, T., Donau, O.K., Plishka, R.J., Buckler-White, A., Martin, M.A., 2004. Induction of disease by a molecularly cloned highly pathogenic simian immunodeficiency virus/human immunodeficiency virus chimera is multigenic. J. Virol. 78, 5513–5519.

Sagar, M., Wu, X., Lee, S., Overbaugh, J., 2006. Human immunodeficiency virus type 1 V1-V2 envelope loop sequences expand and add glycosylation sites over the course of infection, and these modifications affect antibody neutralization sensitivity. J. Virol. 80 (19), 9586–9598.

Shibata, R., Kawamura, M., Sakai, H., Hayami, M., Ishimoto, A., Adachi, A., 1991. Generation of a chimeric human and simian immunodeficiency virus infectious to monkey peripheral blood mononuclear cells. J. Virol. 65 (7), 3514–3520.

Shimizu, Y., Okoba, M., Yamazaki, N., Goto, Y., Miura, T., Hayami, M., Hoshino, H., Haga, T., 2006. Construction and in vitro characterization of a chimeric simian and human immunodeficiency virus with the RANTES gene. Microbes. Infect. 8 (1), 105–113.

Shinohara, K., Sakai, K., Ando, S., Ami, Y., Yoshino, N., Takahashi, E., Someya, K., Suzaki, Y., Nakasone, T., Sasaki, Y., Kaizu, M., Lu, Y., Honda, M., 1999. A highly pathogenic simian/human immunodeficiency virus with genetic changes in cynomolgus monkey. J. Gen. Virol. 80, 1231–1240.

Shiver, J.W., Fu, T.M., Chen, L., Casimiro, D.R., Davies, M.E., Evans, R.K., Zhang, Z.Q., Simon, A.J., Trigona, W.L., Dubey, S.A., Huang, L., Harris, V.A., Long, R.S., Liang, X., Handt, L., Schleif, W.A., Zhu, L., Freed, D.C., Persaud, N.V., Guan, L., Punt, K.S., Tang, A., Chen, M., Wilson, K.A., Collins, K.B., Heidecker, G.J., Fernandez, V.R., Perry, H.C., Joyce, J.G., Grimm, K.M., Cook, J.C., Keller, P.M., Kresock, D.S., Mach, H., Troutman, R.D., Isopi, L.A., Williams, D.M., Xu, Z., Bohannon, K.E., Volkin, D.B., Montefiori, D.C., Miura, A., Krivulka, G.R., Lifton, M.A., Kuroda, M.J., Schmitz, J.E., Letvin, N.L., Caulfield, M.J., Bett, A.J., Youil, R., Kaslow, D.C., Emini, E.A., 2002. Replication-incompetent adenoviral vaccine vector elicits effective anti-immunodeficiency-virus immunity. Nature 415 (6869), 331–335.

Sing, T., Low, A.J., Beerenwinkel, N., Sander, O., Cheung, P.K., Domingues, F.S., Büch, J., Däumer, M., Kaiser, R., Lengauer, T., Harrigan, P.R., 2007. Predicting HIV coreceptor usage on the basis of genetic and clinical covariates. Antivir. Ther. 12 (7), 1097–1106.

Tan, R.C., Harouse, J.M., Gettie, A., Cheng-Mayer, C., 1999. In vivo adaptation of SHIV (SF162): chimeric virus expressing a NSI, CCR5-specific envelope protein. J. Med. Primatol. 28 (4-5), 164–168.

Trkola, A., Kuhmann, S.E., Strizki, J.M., Maxwell, E., Ketas, T., Morgan, T., Pugach, P., Xu, S., Wojcik, L., Tagat, J., Palani, A., Shapiro, S., Clader, J.W., McCombie, S., Reyes, G.R., Baroudy, B.M., Moore, J.P., 2002. HIV-1 escape from a small molecule, CCR5-specific entry inhibitor does not involve CXCR4 use. Proc. Natl. Acad. Sci. U.S.A. 99, 395–400.

Veazey, R.S., DeMaria, M., Chalifoux, L.V., Shvetz, D.E., Pauley, D.R., Knight, H.L., Rosenzweig, M., Johnson, R.P., Desrosiers, R.C., Lackner, A.A., 1998. Gastrointestinal tract as a major site of CD4+ T cell depletion and viral replication in SIV infection. Science 280 (5362), 427–431.

Wei, X., Decker, J.M., Wang, S., Hui, H., Kappes, J.C., Wu, X., Salazar-Gonzalez, J.F., Salazar, M.G., Kilby, J.M., Saag, M.S., Komarova, N.L., Nowak, M.A., Hahn, B.H., Kwong, P.D., Shaw, G.M., 2003. Antibody neutralization and escape by HIV-1. Nature 422 (6929), 307–312.

Willey, R.L., Smith, D.H., Lasky, L.A., Theodore, T.S., Earl, P.L., Moss, B., Capon, D.J., Martin, M.A., 1988. In vitro mutagenesis identifies a region within the envelope gene of the human immunodeficiency virus that is critical for infectivity. J. Virol. 62 (1), 139–147.

Yamaguchi-Kabata, Y., Yamashita, M., Ohkura, S., Hayami, M., Miura, T., 2004. Linkage of amino acid variation and evolution of human immunodeficiency virus type 1 gp120 envelope glycoprotein (subtype B) with usage of the second receptor. J. Mol. Evol. 58 (3), 333–340.

Zhang, Y., Lou, B., Lal, R.B., Gettie, A., Marx, P.A., Moore, J.P., 2000. Use of inhibitors to evaluate coreceptor usage by simian and simian/human immunodeficiency viruses and human immunodeficiency virus type 2 in primary cells. J. Virol. 74 (15), 6893–6910.

WEB REFERENCES

Web PSSM, Mullins Lab, University of Washington http://indra.mullins.microbiol.washington.edu/webpssm/

Geno2pheno [coreceptor], Max-Planck-Institut Informatik. http://coreceptor.bioinf.mpi-inf.mpg.de

Please cite this article as: Matsuda, K., et al., *In vivo* analysis of a new R5 tropic SHIV generated from the highly pathogenic SHIV-KS661, a derivative of SHIV-89.6, Virology (2010), doi:10.1016/j.virol.2010.01.008

«paper no. vir017368 charlesworth ref: vir017368»

Animal RNA

Journal of General Virology (2010), 91, 000–000 DOI 10.1099/vir.0.017368-0

Small intestine CD4$^+$ cell reduction and enteropathy in simian/human immunodeficiency virus KS661-infected rhesus macaques in the presence of low viral load

Katsuhisa Inaba,[1] Yoshinori Fukazawa,[1] Kenta Matsuda,[1] Ai Himeno,[1] Megumi Matsuyama,[1] Kentaro Ibuki,[1] Yoshiharu Miura,[2] Yoshio Koyanagi,[2] Atsushi Nakajima,[3] Richard S. Blumberg,[4] Hidemi Takahashi,[5] Masanori Hayami,[1] Tatsuhiko Igarashi[1] and Tomoyuki Miura[1]

Correspondence
Tomoyuki Miura
tmiura@virus.kyoto-u.ac.jp

[1]Laboratory of Primate Model, Experimental Research Center for Infectious Diseases, Institute for Virus Research, Kyoto University, 53 Shogoinkawaramachi, Sakyo-ku, Kyoto 606-8507, Japan

[2]Laboratory of Viral Pathogenesis, Institute for Virus Research, Kyoto University, 53 Shogoinkawaramachi, Sakyo-ku, Kyoto 606-8507, Japan

[3]Division of Gastroenterology, Yokohama City University Graduate School of Medicine, Yokohama, Japan

[4]Division of Gastroenterology, Brigham and Women's Hospital, Harvard Medical School, Boston, MA, USA

[5]Department of Microbiology and Immunology, Nippon Medical School, Tokyo, Japan

Human immunodeficiency virus type 1, simian immunodeficiency virus and simian/human immunodeficiency virus (SHIV) infection generally lead to death of the host accompanied by high viraemia and profound CD4$^+$ T-cell depletion. SHIV clone KS661-infected rhesus macaques with a high viral load set point (HVL) ultimately experience diarrhoea and wasting at 6–12 months after infection. In contrast, infected macaques with a low viral load set point (LVL) usually live asymptomatically throughout the observation period, and are therefore referred to as asymptomatic LVL (Asym LVL) macaques. Interestingly, some LVL macaques exhibited diarrhoea and wasting similar to the symptoms of HVL macaques and are termed symptomatic LVL (Sym LVL) macaques. This study tested the hypothesis that Sym LVL macaques have the same degree of intestinal abnormalities as HVL macaques. The proviral DNA loads in lymphoid tissue and the intestines of Sym LVL and Asym LVL macaques were comparable and all infected monkeys showed villous atrophy. Notably, the CD4$^+$ cell frequencies of lymphoid tissues and intestines in Sym LVL macaques were remarkably lower than those in Asym LVL and uninfected macaques. Furthermore, Sym LVL and HVL macaques exhibited an increased number of activated macrophages. In conclusion, intestinal disorders including CD4$^+$ cell reduction and abnormal immune activation can be observed in SHIV-KS661-infected macaques independent of virus replication levels.

Received 5 October 2009
Accepted 3 November 2009

INTRODUCTION

The intestinal tract, which is the largest mucosal and lymphoid organ and which contains the majority of the total lymphocytes in the body, is an important port of entry for human immunodeficiency virus type 1 (HIV-1) infection in vertical and homosexual transmission (Smith *et al.*, 2003). Additionally, the intestinal tract is a central site in the interaction between HIV-1 and its host, and suffers profound pathological changes as a result of HIV-1 infection. HIV-1 infection of the intestinal tract is characterized by virus replication (Fackler *et al.*, 1998), CD4$^+$ T-cell depletion (Brenchley *et al.*, 2004), opportunistic infection and HIV enteropathy, which is an idiopathic intestinal disorder observed in infected patients with diarrhoea (Kotler, 2005). In particular, CD4$^+$ T-cell depletion, which is the immunological hallmark in the development of AIDS, preferentially takes place in the intestinal tract rather than in the peripheral blood throughout the infection (Brenchley *et al.*, 2004). This observation is based on the following findings: (i) most

naturally transmitted HIV-1 strains are chemokine receptor 5 (CCR5)-tropic; and (ii) the intestinal tract, especially the lamina propria, contains a large number of activated memory $CCR5^+$ $CD4^+$ T cells, which indicates a high susceptibility for HIV-1 infection, whereas the peripheral blood has a relatively small population of these cells (Anton *et al.*, 2000; Lapenta *et al.*, 1999). $CD4^+$ T-cell depletion from the intestinal tract by HIV-1 infection is thought to lead to progressive dysfunction of mucosal immunity, which triggers immunodeficiency (Paiardini *et al.*, 2008). In addition to $CD4^+$ T-cell depletion in the intestinal tract, HIV-1 infection causes histopathological changes in the intestine, including villous atrophy, crypt hyperplasia and acute/chronic inflammation (Batman *et al.*, 1989).

Chronic disease of the intestinal tract generally manifests as inflammation (Kahn, 1997). Diarrhoea is a major intestinal symptom caused by various stimuli to the intestinal tract such as pathogens, toxins and dysfunction of the immune system (Gibbons & Fuchs, 2007). Because HIV-1 infection weakens the host immune system, AIDS is one of the primary causes of chronic diarrhoea (Sestak, 2005). In developing countries, diarrhoea was a major symptom in advanced HIV-1 infection prior to the establishment of highly active antiretroviral therapy (HAART) (Wilcox & Saag, 2008). Dehydration and malabsorption as a result of chronic diarrhoea can lead to progressive weight loss and can contribute to morbidity and mortality in HIV-1-infected patients (Sharpstone & Gazzard, 1996). Therefore, chronic diarrhoea is one of the most important clinical signs in AIDS patients.

AIDS models using non-human primates have provided many important observations on AIDS pathogenesis. The first finding of early $CD4^+$ T-cell depletion from the intestinal tract was reported in a study using simian immunodeficiency virus (SIV)-infected macaques (Veazey *et al.*, 1998). Intestinal $CD4^+$ T cells of rhesus macaques predominantly exhibit a $CCR5^+$ activated memory phenotype, and $CD4^+$ T cells of this phenotype are selectively eliminated in SIV-infected macaques, indicating that the majority of intestinal $CD4^+$ T cells are primary targets of SIV infection (Veazey *et al.*, 2000a, b). Accordingly, detailed analysis of the intestinal tract using animal models is essential for an understanding of AIDS pathogenesis.

Simian/human immunodeficiency virus (SHIV)-KS661 is a molecular clone and a pathogenic virus in rhesus macaques. SHIV-KS661 systemically depletes $CD4^+$ T cells of rhesus macaques within 4 weeks of infection (Miyake *et al.*, 2006). Based on our observations over a number of years, intravenous infection of rhesus macaques with SHIV-KS661 consistently results in high viraemia and $CD4^+$ T-cell depletion, followed by malignant morbidity as a result of severe chronic diarrhoea and wasting after 6–18 months. Generally, the time to clinical morbidity in rhesus macaques infected with pathogenic SHIVs, such as SHIV-89.6P and SHIV-KS661, is considerably shorter than in HIV-1-infected humans, who take an average of 10 years to progress to AIDS. In addition, all subsets of $CD4^+$ T cells including memory and naïve T cells are thoroughly depleted in pathogenic SHIV-infected macaques. However, in the SHIV-KS661 macaque model, diarrhoea and wasting, which are major symptoms in advanced HIV-1 infection, can clearly be recognized and defined in association with disease progression.

Recently, we observed that, in many rhesus macaques infected intrarectally with SHIV-KS661, plasma viral RNA loads decreased gradually to undetectable levels in the chronic phase, which is quite different from the case with intravenous infection. It is well known that pathogenic SIV and SHIV infections in monkeys, like HIV-1 infections in humans, generally lead to high viraemia, profound $CD4^+$ T-cell depletion and death. Interestingly, in this study, two out of six intrarectally inoculated macaques with a low plasma viral load experienced malignant morbidity manifest as severe diarrhoea and wasting, similar to what we observed in infected macaques with high viraemia. The purpose of this study was to elucidate why macaques with a low plasma viral load experienced diarrhoea and wasting. As an explanation for this morbidity, we hypothesized that, even if the viral load set-point is suppressed, SHIV-KS661-infected macaques would have the same degree of intestinal abnormalities as infected macaques with high viraemia. To test this hypothesis, we analysed $CD4^+$ cell frequencies in lymphoid and intestinal tissues and damage to the intestinal mucosa in infected macaques with high and low viral load set points (HVL and LVL, respectively). Here, we have provided evidence for the development of intestinal disorders in SHIV-KS661-infected macaques irrespective of the plasma viral RNA load.

RESULTS

Diarrhoea and wasting in two macaques despite low viral load

All macaques inoculated intravenously with SHIV-KS661 and one out of seven macaques inoculated intrarectally with SHIV-KS661 exhibited high set points of plasma viral RNA loads, persisting at over 10^6 copies ml^{-1} until they needed to be euthanized as a result of diarrhoea and wasting (Fig. 1a). In contrast, in the remaining six macaques inoculated intrarectally with SHIV-KS661, the set points of plasma viral RNA load gradually decreased to undetectable levels (Fig. 1a). We called these macaques showing high and low set points of viral RNA load HVL and LVL macaques, respectively. During an observation period of approximately 1.4 years, two LVL macaques (MM397 and MM399) experienced severe diarrhoea and wasting and required euthanasia at approximately 22 weeks post-infection (p.i.), similar to HVL macaques, whereas the remaining four LVL macaques were asymptomatic (Fig. 1a). We termed the healthy LVL macaques asymptomatic LVL macaques (Asym LVL) and the LVL